DEPARTMENT OF THE NAVY

HYDROMECHANICS

O

AERODYNAMICS

O

STRUCTURAL MECHANICS

O

APPLIED MATHEMATICS

O

ACOUSTICS AND VIBRATION

COOPERATIVE ROTATING-ARM AND STRAIGHT-LINE EXPERIMENTS WITH ITTC STANDARD MODEL (MARINER TYPE SHIP)

by

Morton Gertler

The distribution of this report is unlimited

HYDROMECHANICS LABORATORY
RESEARCH AND DEVELOPMENT REPORT

June 1966 Report No. 2221

COOPERATIVE ROTATING-ARM AND STRAIGHTLINE EXPERIMENTS WITH ITTC STANDARD MODEL (MARINER TYPE SHIP)

by

Morton Gertler

JUNE 1966

REPORT 2221
SR 009 01 01
Task 0102

TABLE OF CONTENTS

LIST OF FIGURES

Page

LIST OF TABLES

NOTATION

The following nomenclature is in accordance with the standards adopted by the Tenth International Towing Tank Conference September 1963:

Symbol	Dimensionless Form	Definition
D		Propeller diameter
	$F_n = \frac{U}{\sqrt{gL}}$	Froude number
	$J = \frac{U}{nD}$	Propeller advance coefficient
L	$L' = 1$	Length of ship (in this report length between perpendiculars)
n		Propeller frequency of revolution
N	$N' = \frac{N}{\frac{1}{2}\rho L^3 U^2}$	Hydrodynamic yawing moment
N_r	$N_r' = \frac{N_r}{\frac{1}{2}\rho L^4 U}$	Derivative of yawing moment component with respect to angular velocity component r
N_v	$N_v' = \frac{N_v}{\frac{1}{2}\rho L^3 U}$	Derivative of yawing moment component with respect to linear velocity component v
$N_{\delta R}$	$N_{\delta R}' = \frac{N_{\delta R}}{\frac{1}{2}\rho L^3 U^2}$	Derivative of yawing moment component with respect to rudder angle component δ_R
r	$r' = \frac{rL}{U}$	Yawing angular velocity component
U	$U' = 1$	Velocity of origin of body axes relative to fluid

v	$v' = \frac{v}{U}$	Component along y-axis of velocity of origin of body axes relative to fluid
X	$X' = \frac{X}{\frac{1}{2}\rho L^2 U^2}$	Hydrodynamic longitudinal force, positive forward
x		Longitudinal axis, directed from after to forward end of ship with origin at center of gravity
Y	$Y' = \frac{Y}{\frac{1}{2}\rho L^2 U^2}$	Hydrodynamic lateral force, positive to starboard
Y_r	$Y_r' = \frac{Y_r}{\frac{1}{2}\rho L^3 U}$	Derivative of lateral force component with respect to angular velocity component r
Y_v	$Y_v' = \frac{Y_v}{\frac{1}{2}\rho L^2 U}$	Derivative of lateral force component with respect to linear velocity component v
$Y_{\delta R}$	$Y_{\delta R}' = \frac{Y_{\delta R}}{\frac{1}{2}\rho L^2 U^2}$	Derivative of lateral force component with respect to rudder angle component δ_R
y		Distance along transverse axis, directed to starboard with origin at center of gravity
β		Angle of drift
δ_R		Rudder angle
θ		Pitch angle (with respect to horizontal plane)
ϕ		Roll angle (with respect to vertical plane)

ABSTRACT

Pursuant to the ITTC Maneuverability Committee's Cooperative Program, the David Taylor Model Basin has carried out an extensive series of rotating-arm and straightline experiments with a 22-foot long standard model (MARINER Type Ship). This report describes in detail the model, apparatus, and techniques used in the investigation and presents the experimental results in both tabular and graphical form as nondimensional hydrodynamic coefficients and as stability and control derivatives. It is concluded that, if the same model, instrumentation, test procedures, and initial conditions are used, the same numerical values can be obtained for the individual static stability and control derivatives from rotating-arm tests as from straightline tests.

INTRODUCTION

The experimental investigation reported herein is part of the David Taylor Model Basin's contribution to the ITTC Maneuverability Committee's Cooperative Program[1] dealing with techniques for determining the maneuverability characteristics of surface ships. The primary purpose of this report is to present the data that have been obtained by means of rotating-arm and straightline tests with the ITTC Standard Model (MARINER Type Ship) along with a detailed description of the associated facilities, instrumentation, and test techniques employed in the investigation. The data are presented in a form which should facilitate direct comparisons with similar data provided by other participants of the Cooperative Program. The use of these data in analog or digital computer studies to make predictions for and to establish correlations with the full-scale MARINER type ship[2] will form the subject of a future report.

The ITTC Maneuverability Committee's Cooperative Program was established in 1962-63. The objective of the first phase of the program is to establish the extent to which agreement exists between the data produced by the various laboratories using each of several alternative model test techniques. To accomplish this objective, the Committee selected the MARINER type ship as the "Standard Model", furnished the participating laboratories with a complete set of lines plans, and outlined the standard conditions to be adhered to in the model tests. Each organization was free to construct a model of a size compatible with its own facilities and to conduct the cooperative tests using its own instrumentation and techniques.

The types of tests embraced by the Cooperative Program fall into two general categories called "free-running-model" and "captive-model" tests, respectively. The term free-running-model test is applied to the well-known class of experiments in which maneuvers are performed with dynamically-scaled models that are self-propelled without external restraint, and the resulting motions or trajectory data are recorded. The models can be cable-controlled, radio-controlled, or manned vehicles. The term captive-model tests is used to denote the type of experiment in which the model is constrained,

[1] References are listed on page 34.

usually to a towing carriage, and the forces and moments used to determine the numerical values of the hydrodynamic coefficients for the equations of motions are measured. Included in this category are: straightline yawed-flight tests, rotating-arm tests, and planar-motion-mechanism or oscillation tests.

The Model Basin's participation in the Cooperative Program extends to both categories of tests. Free-running tests with a radio-controlled model have already been conducted in the Maneuvering and Seakeeping Facility using a large (about 22-foot long) model of MARINER. A separate report, containing a complete account of these tests, is being prepared and a portion of the data has been issued.[3] In the captive-model category, the subject rotating-arm and straightline tests were conducted with the same model and some comparative data have been issued.[4] However, since the DTMB Planar-Motion-Mechanism System has not yet been adapted to test surface-ship models, the remaining part of the captive-model program will be reported separately.

This report describes the model, apparatus, and techniques used in the experiments conducted by the Model Basin for the ITTC Maneuverability Committee's Cooperative Program; outlines the procedures used in the reduction and presentation of the experimental data; discusses the quality of the data from the standpoint of scatter and repeatability; compares the rotating-arm test data with corresponding straightline test data; briefly compares the stability and control derivatives obtained from the subject tests with those obtained by some of the other participants of the Cooperative Program; and draws some conclusions concerning relative merits of the two techniques from the standpoint of determining the various hydrodynamic coefficients required for the equations of motion of surface ships.

DESCRIPTION OF MODEL AND PROTOTYPE

The MARINER Type Ship was selected for the "ITTC Standard Model" because its configuration is considered to be typical of modern commercial ships. Furthermore, extensive full-scale maneuvering data are available for this type of ship[2] making it even more desirable for the intended purpose. The configuration of the ship is shown by the lines plans given in Figure 1. The pertinent geometrical characteristics are listed in Table 1 in terms of model and ship dimensions.

As specified by the ITTC Maneuverability Committee, the configuration of the Standard Model is identical with that for the MARINER Type Ship described in Reference 5. However, both its displacement and trim correspond to the conditions that existed during the full-scale trials of COMPASS ISLAND[2]. Thus, the configuration of the Standard Model differs from that for which full-scale trial data are available in two respects: the bilge keels are longer (110 feet compared with 62.5 feet) and there is no sonar dome.

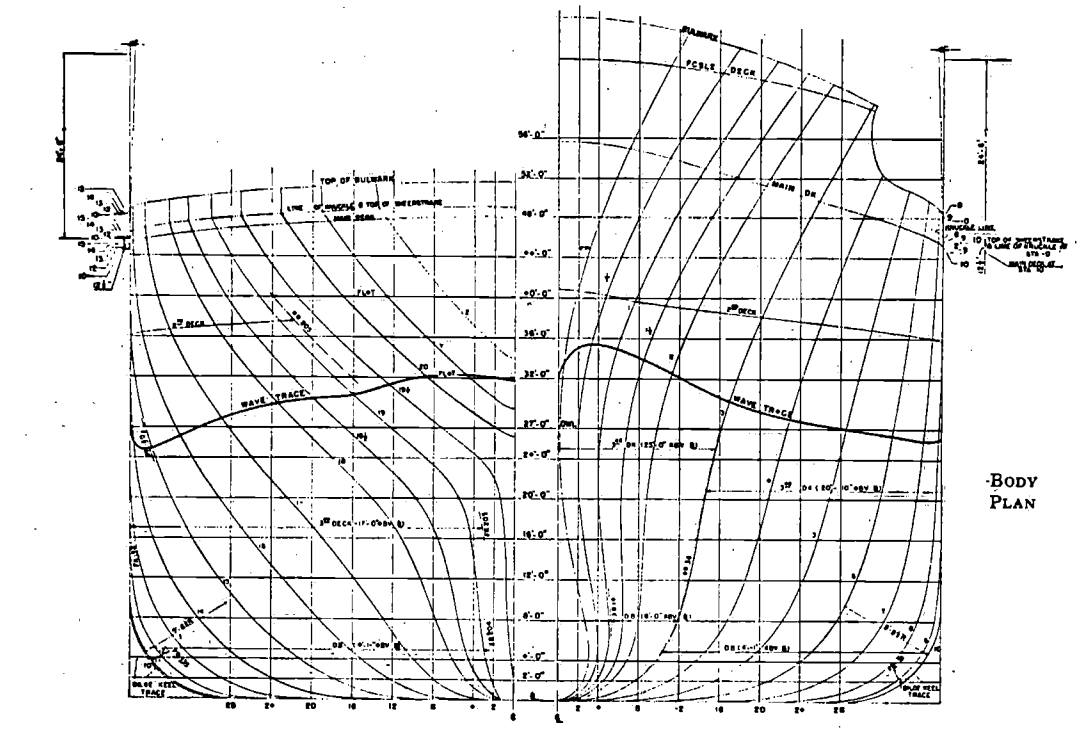

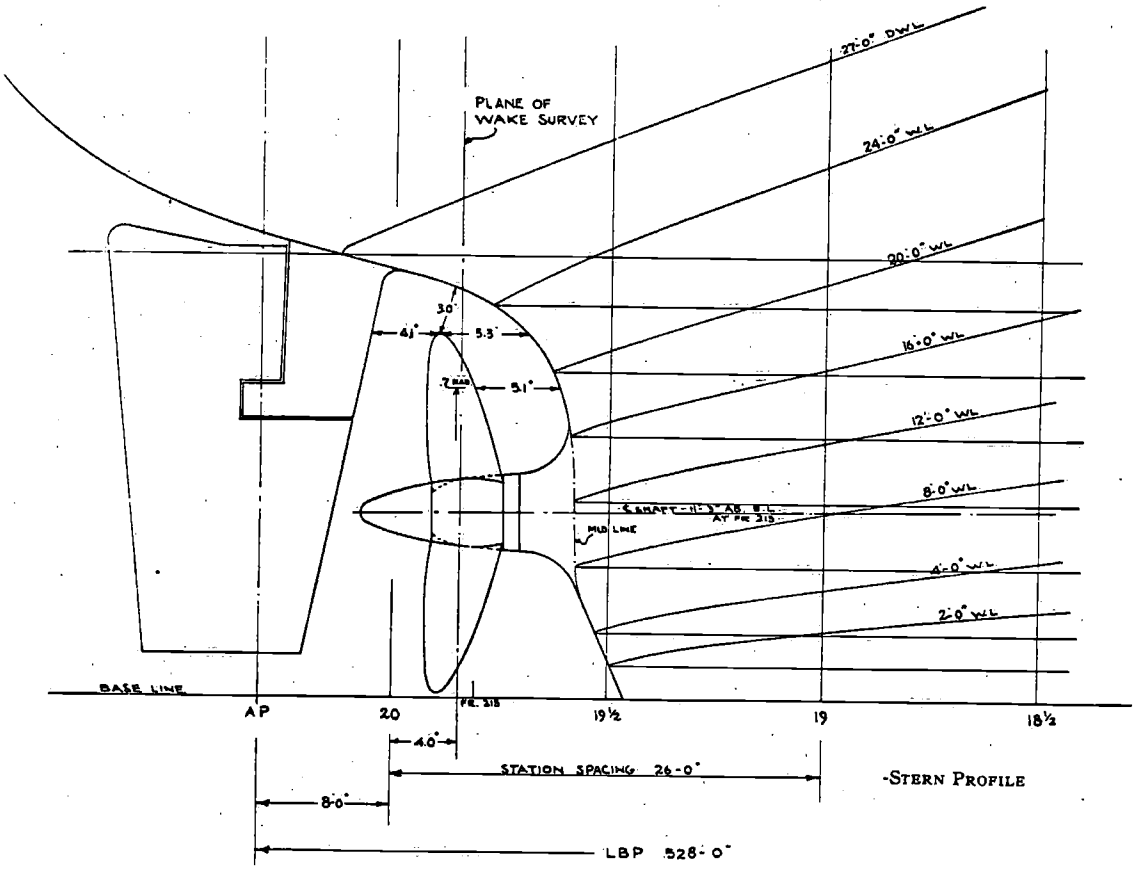

Figure 1 - Lines of ITTC Standard Model (MARINER Type Ship)

TABLE 1

Geometric Characteristics of ITTC Standard Model and Prototype
(MARINER Type Ship)

Ship	MARINER
Model No.	4414
Model Propeller No.	3249
Linear Ratio, λ	24.175
Lines Plan	Bethlehem Steel Corp. No.
Bow	CTD C4-S-1a-H15A, Alt 1
Stern	CTD C4-S-1a-H15B, Alt 4
Appendage Plan No.	
Rudder	C4-S-1a-H150, Alt 4
Bilge Keels	CTD-C4-S-1a-H-70 and C4-S1A-123-5 Alt III and offsets

	Ship	Model
Hull		
Length Between Perpendiculars, ft.	528.00	21.841
Beam, ft.	76.00	3.144
Mean Draft, ft.	24.50	1.013
Trim by Stern, ft.	4.00	0.165
Displacement, tons, lbs	16800.	2590.0
Nominal Center of Gravity Location		
Distance Aft of Station 10, ft.	6.90	0.285
Height Above Baseline, ft.	25.40	1.051
Length-Beam Ratio	6.947	6.947
Beam-Draft Ratio	3.102	3.102
Displacement-Length Ratio	114.13	114.13
Prismatic Coefficient	0.6246	0.6246
Block Coefficient	0.6125	0.6125
Rudder (Semi-Balanced)		
Mean Chord, ft	13.08	0.541
Span, ft.	24.00	0.993
Total Projected Area, ft^2	314.00	0.5373
Movable Projected Area, ft^2	271.84	0.4651
Aspect Ratio	1.834	1.834
Percent Balance	20.91	20.91
Rudder Area Coefficient	0.0224	0.0224
Maximum Design Rudder Angle, deg	40.0	40.0
Rudder Rate, deg/sec	2.5 to 3.7	-
Propeller		
Direction of Rotation	RH	RH
Number of Blades	4	4
Pitch, ft.	22.83	0.945
Diameter, ft.	22.00	0.910
Pitch-Diameter Ratio	0.964	0.964
Expanded Area Ratio	0.565	0.563
Bilge Keels		
Length, ft.	110.00	4.550
Depth, ft.	1.50	0.062

NOTE: Rudder dimensions are based on immersed portion for specified displacement and trim

DTMB Model 4414 was used for the entire experimental investigation covered by this report. The model is about 22 feet long, constructed of sugar pine, and painted with enamel to achieve a smooth surface finish. To fulfill the objectives of the Cooperative Program, the underwater portion of the model, including hull, propeller, rudder and bilge keels was made geometrically similar, in every respect possible, to the Standard Model specified by the Maneuverability Committee. The model was equipped with an electric motor to drive the propeller and a rotary actuator to swing the rudder. The force balances and other measuring equipment, described later in this report, were installed in the model and supplementary lead ballast weights were used to achieve the specified displacement and trim conditions.

TEST APPARATUS

The two major facilities that were used for the subject investigation at the David Taylor Model Basin are the Rotating-Arm Facility and the Deep-Water Towing Basin. The Rotating Arm Facility is described in detail in Reference 6. It consists of a circular basin, 260 feet in diameter with a water depth of 20 feet, and a radial towing arm. The towing arm is essentially a Parker truss which pivots about a bearing on a center island. It is supported at two points by virtue of the bearing at the center pivot and the wheels on the peripheral tracks. The Deep-Water Basin, described in Reference 7, is a conventional straightline towing basin. It has a rectangular cross-section with a width of 52 feet and a water depth of 22 feet. The portion of the basin used for the investigation is spanned by Towing Carriage 2 and extends for a length of about 1780 feet.

The towing arrangement and measuring apparatus used for the experiments are shown schematically in Figure 2. To facilitate direct comparison of the two different experimental techniques, not only the model, but the towing arrangement and other equipment used for the tests in the two facilities were deliberately made identical.

The towing apparatus shown by Figure 2 was assembled from existing parts used in connection with other model tests. Since the major quantities to be determined were the hydrodynamic coefficients associated with the equations of motion defining horizontal-plane maneuvers, it was decided that the model should be held captive in those modes where forces and moments were to be measured and free to assume the appropriate underwater configuration in the remaining modes. This was accomplished by arranging the towing apparatus so that the model is restrained in yaw, sidesway, and surge but is free to pitch, heave, and roll. As indicated by the sketch, the pin-joints in combination with the gimbals on the towing linkages allow the model to both pitch and heave. The gimbals, which are associated with the gage system, permit movement in three degrees of freedom about their own individual axes. However, collectively they provide restraint in yaw, sidesway and surge, but allow movement in roll since their longitudinal axes are coincident. The model can be locked out in roll, if desired, by inserting a locking pin into the roll balance contained in one of the gimbals.

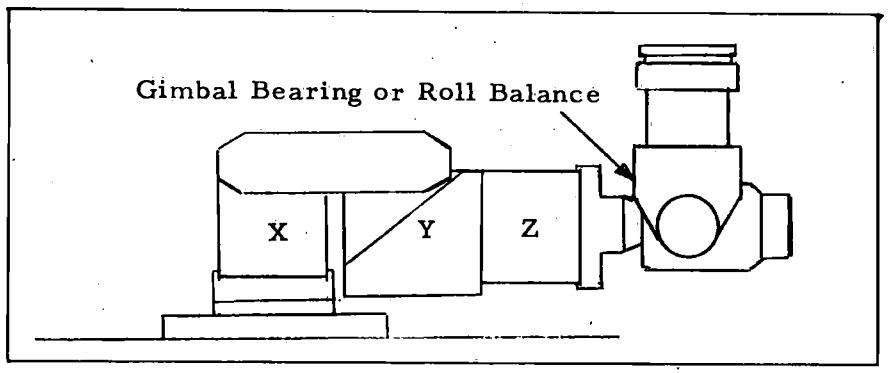

Enlarged View of a Gage Assembly

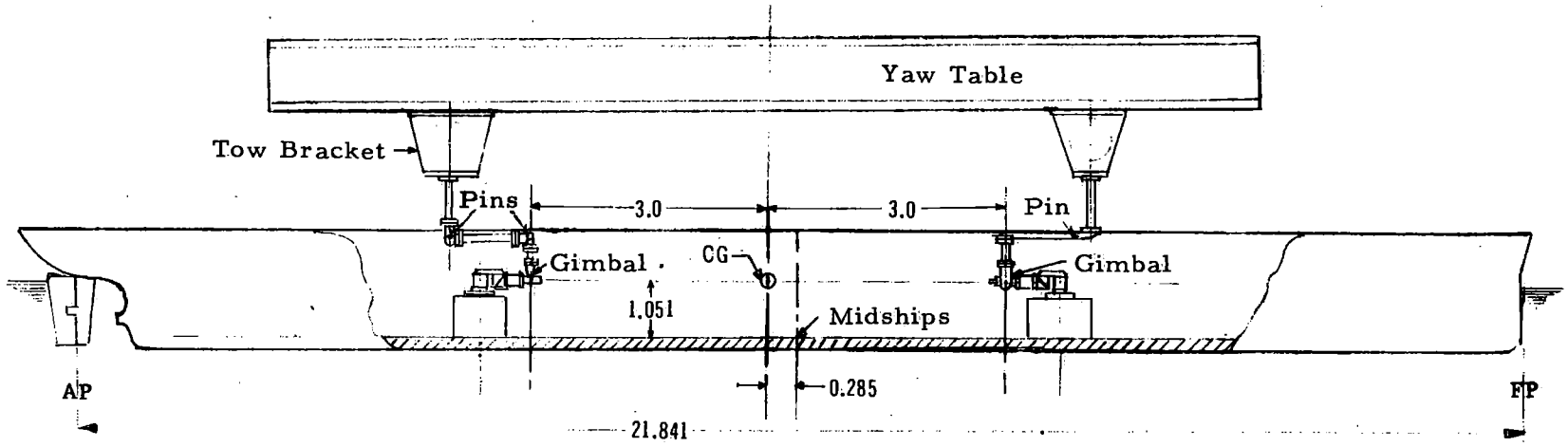

Figure 2 - Schematic Sketch of Towing Arrangement and Measuring Apparatus
(All dimensions are in feet)

The gage system and associated recording equipment is described in detail in Reference 8. It is essentially the same as that used with the DTMB Planar-Motion-Mechanism System. As seen in the enlarged view of Figure 2, each gage assembly consists of three modular force gages, connected in series and oriented to measure X-, Y-, and Z-forces together with either a gimbal or roll balance. Since the model is free to pitch and heave in the subject experiments, the Z-gage is used merely as a spacer. Also, the roll balance is inactive because the locking pin is removed and the model is free to roll. One end of each gage assembly is attached to the model by means of a baseplate; the other end is attached to the yaw table through the tow bracket. Thus, the total weight of all of the components of the gage system, up to and including about half the horizontal member of each towing linkage, becomes part of the model ballast.

The gage assemblies are located in the model so that they measure components of force referred to a body-axis system having as its origin the center of gravity of the ship (see Table 1). The gimbal centers are spaced equidistant (±3.0 feet) from either side of the reference point; the gages sense pure reaction forces at each gimbal center and the moment about these gimbal centers is zero. It should be mentioned that the individual gages do not sense the portion of the inertial forces due to the weight of the parts of the system between the center of the gage and the center of the horizontal member of the towing linkage. These weights have been calculated and confirmed experimentally to be 131.5 pounds and 181.0 pounds up to the centers of the pair of Y-gages and the pair of X-gages, respectively. In each case, the weight involved amounts to roughly 5 percent of the model displacement. Therefore, it is necessary to make appropriate corrections to the measured X and Y forces, as explained in a later section of this report.

The devices for setting and reading out the various angles are not shown by the sketch in Figure 2. The rudder angles can be set and read out remotely on the towing carriage by means of an electric rotary actuator which contains a potentiometer which is calibrated over a range of ±45 degrees. The yaw (drift) angles are set by rotating the model-yaw table combination, about a central bearing, with respect to the towing carriage. Somewhat different arrangements are used for this purpose on the two facilities. On Carriage 2, the yaw angles are set manually by inserting a positioning pin and heavy bolt into previously indexed holes in plates between the yaw table and towing carriage. On the Rotating Arm, the yaw table is motor-driven by, and operates in parallel with the angle-positioning device permanently installed on the facility.[6] The angles are sensed on this device by a mechanical read-out digital counter installed at the motor end of the gear train. Thus, the yaw angles can be both set and read out at the instrument console on the Rotating Arm. The pitch and roll angles assumed by the model during the course of the experiments on both facilities are sensed and read out by a Minneapolis Honeywell Vertical Gyroscope. The propeller rpm is sensed and read out by means of a tachometer generator.

On the Rotating Arm, the radius settings are made by means of the sub-carriage which is moved radially along a pair of rails by a windlass and cable. The precise setting is obtained manually by inserting four 1-inch-diameter pins, one at each of the four corners of the sub-carriage, into index holes on the rail. The pins also serve as strength members to hold the carriage in place.

The measurements obtained with the foregoing instrumentation are recorded during the tests by means of the digital recording system described in detail in Reference 8. The recording equipment is located in the Instrument Penthouse in the case of Carriage 2 and at an instrument console in the case of the Rotating Arm.

TEST PROCEDURE

Prior to conducting a given series of tests for the formal program, the model was carefully ballasted and trimmed as follows:

The fully ballasted model (including all instrumentation and equipment contributing to its weight) was first weighed on a platform scale. While weighing, the towing linkages and electric cables were supported so that the model weight (or displacement) was precisely the same as it would be when attached to the towing carriage. The model was then put into the water and the ballast weights were moved longitudinally to obtain the correct trim, as indicated by draft marks; transversely to obtain zero heel, as indicated by a level placed across the top lift of the model; and vertically to obtain the correct height for the center of gravity, as indicated by moment-to-trim tests. Insofar as could be determined, the resulting conditions for the model at rest in the water were identical to those listed in Table 1. Since captive-model tests of the steady-state variety were to be conducted, no attempt was made to swing the model to obtain the radii of gyration.

In addition, all of the measuring instruments were carefully calibrated prior to the tests. The modular force gages were individually calibrated with standardized weights; the vertical gyroscope was calibrated in roll and pitch on a tilt table, the rudder angle sensor was calibrated by setting the rudder at discrete angles (as indicated by a protractor) with respect to a centerline scribed on the model; and the tachometer generator used to measure propeller rpm was calibrated with a synchronous motor.

The general procedure used for the formal tests in the two facilities are as follows:

With the model attached to the towing carriage and at rest, the digital recorders are balanced and adjusted to read zero for zero force on the modular gages and zero angles on the vertical gyroscope, rudder, and yaw table

(Rotating Arm only). Then, for any given model setting of yaw angle, rudder angle, and turning radius, the model is brought up to a predetermined speed corresponding on Froude scaling to the full-scale approach speed. At the same time, the propeller speed is adjusted to an rpm corresponding to the point of propulsion of the full-scale ship for the given speed. When essentially steady conditions are reached, as indicated by the readings on the digital recorder, the run is maintained for at least 10 seconds. The recorder is then put on "hold" and the readings which represent average steady-state values are transferred to the data sheet by an automatic typewriter.[8] At the end of a run or series of runs, the model is towed slowly back to the starting position in the basin. A waiting period of at least 12 minutes duration between the beginning of successive runs is taken to allow the water in the basin to become free of waves and currents.

The rotating-arm tests were run at approach speeds (tangential velocities) of 4.06 and 2.03 knots corresponding to 20 and 10 knots full-scale, respectively. At each speed, the propeller rpm was adjusted to correspond to the specified point of propulsion (for full-scale ship proceeding on straight course). The rpm was based on the results of propulsion tests conducted on the same MARINER model rather than that presented for COMPASS ISLAND in Reference 2. To avoid operating in a current generated by the wake of the model, each run was completed within one revolution of the Rotating Arm. Consequently, it was not practical to attempt to obtain reliable measurements for more than one model setting during any one run.

The most complete set of tests on the Rotating Arm was carried out for the 20-knot condition. The sequence of tests for this condition is summarized by Table 2.

In each group of tests listed in Table 2, two of the parameters were held constant while the third was varied in discrete increments over the range shown. Groups 1R, 2R, and 3R are considered to be reference tests. They were designed to permit as direct determination of the stability and control derivatives Y_v', N_v', Y_{δ_R}', N_{δ_R}', Y_r', and N_r' as possible with a facility of this type, and also to enable direct comparisons to be made with similar quantities obtained in other facilities or by other techniques. The value of $r' = 0.2045$ used in the reference tests of Groups 1R and 2R was based on the largest radius that could be obtained in the Rotating Arm Facility with the subject model without incurring wall effects. It was hoped that this radius would be large enough to approximate the straightline case ($r' = 0$) from the standpoint of directly determining static stability and control derivatives from the slopes of the Y' and N' versus β-curves and the Y' and N' versus δ_R-curves. The tests in Group 3R were designed to permit direct determination of the derivatives Y_r' and N_r'. The remaining groups of rotating-arm tests were designed to reveal nonlinearities and coupling effects. In addition to the groups of tests shown in Table 2, a special group of tests was conducted on the model without propeller for a condition of $r' = 0.2045$, $\beta = 0$, with δ_R varied between 0 and -35.0 degrees. Also, a few runs were made for a condition of $r' = 0.2045$, $\beta = 0$, and $\delta_R = 0$ with propeller rpm varied to give advanced coefficients J of from 0.652 to 3.931; and for a condition $r' = 0.2045$, $\beta = 0$, and $\delta_R = 35$ deg for values of J of from 0.652 to 0.979.

TABLE 2

Sequence of Rotating-Arm Tests for 20-Knot Condition

Group No.	r'	β degrees	δ_R degrees
1R	0.2045	-5.0 to 18.0	0
2R	0.2045	0	5.0 to -35.0
3R	0.1858 to 0.7757	0	0
4R	0.6246	-5.0 to 20.0	0
5R	0.6246	0	-5.0 to -35.0
6R	0.6246	10.0	-5.0 to -35.0
7R	0.6246	20	-5.0 to -35.0
8R	0.2930	-5.0 to 20.0	0
9R	0.2930	10.0	0 to -35.0
10R	0.2930	20.0	0 to -35.0
11R	0.2045	0	-10.0 to -35.0
12R	0.2045	10.0	0 to -35.0
13R	0.2045	20.0	0 to -35.0

The straightline tests were run at the same approach speeds and propeller rpms as used for the rotating-arm tests. However, due to the length of the straightline basin, it was possible to make from four to six steady-state runs in one complete trip up the basin. Since only the rudder setting was remotely adjustable, the yaw angle setting was made while the model was stationary and the incremental rudder-angle settings were made while the model was proceeding at constant approach speed. The sequence of straightline tests conducted for the 20-knot condition is summarized by Table 3.

TABLE 3

Sequence of Straightline Tests for 20-Knot Condition

Group No.	β degrees	δ_R degrees
1S	0	20.0 to -35.0
2S	5	0 to -35.0
3S	10	0 to -35.0
4S	15	0 to -35.0
5S	-6.4	0 to -35.0
6S	-10	0 to -35.0

Group 1S was conducted as a reference test to permit direct determination of the control derivatives Y_{δ_R}' and N_{δ_R}'. Because of the lack of a remotely adjustable yaw-table, it was considered too time-consuming to make a reference test for the static stability derivatives Y_v' and N_v'. Consequently, it is necessary to obtain these derivatives from the cross-plots of the data obtained from Groups 1S through 6S for the case of $\delta_R = 0$.

REDUCTION AND PRESENTATION OF DATA

The methods used to reduce the data for the Cooperative Program are considered to be reasonably representative of current practices followed at the David Taylor Model Basin in connection with captive-model stability and control tests for surface ships. The procedural steps are as follows:

1. The Y-forces measured as reactions at the gimbal centers by each of two of the modular gages are added vectorially to obtain the total model Y-force.

2. The same two Y-forces are subtracted vectorially and the vector difference is multiplied by the longitudinal distance from one gimbal center to the reference point (CG) to obtain the model N-moment.

3. The X-forces indicated by each of the other two modular gages are added vectorially to give the total X-force.

4. The values of the measured model X-force, Y-force, and N-moment are converted to nondimensional coefficients in accordance with the ITTC Standard Nomenclature given in this report.

5. The force coefficients based on the gage readings are "corrected" to account for instrumentation tare and, in the case of the rotating-arm data, for centrifugal force to obtain the hydrodynamic coefficients X' and Y'. No correction is required for the hydrodynamic yawing moment coefficient N' since the reference point is at the model center of gravity.

The instrumentation tare mentioned in Step 5 results from that portion of the model weight which is not sensed by a given pair of modular gages (see section on Test Apparatus). It is affected both by the angles (roll and pitch) assumed by the model while underway and the centrifugal force exerted on the model during rotating-arm tests. In addition to correcting for its effect on the tare, the usual practice at the Taylor Model Basin is to exclude the centrifugal force entirely when presenting hydrodynamic force coefficients.

In accordance with the foregoing, the corrections made to the force coefficients based on the direct gage readings to obtain the hydrodynamic force coefficients Y' and X' are given by the following expressions:

$$Y' = Y_{GR}' + m_Y' \sin\phi + (m' - m_Y') r' \cos\beta \cos\phi$$

$$= Y_{GR}' + 0.000405 \sin\phi + (0.007978 - 0.000405) r' \cos\beta \cos\phi$$

$$= Y_{GR}' + 0.000405 \sin\phi + 0.007573 r' \cos\beta \cos\phi$$

and

$X' = X_{GR}' - m_X' \sin\theta + (m' - m_X') r' \sin\beta \cos\theta$, or neglecting the effect of θ since its maximum value is 0.6 degree,

$$X' = X_{GR}' + (m' - m_X') r' \sin\beta$$

$$= X_{GR}' + (0.007978 - 0.000557) r' \sin\beta$$

$$= X_{GR}' + 0.007421 r' \sin\beta$$

where

$Y_{GR'}$ is the Y-force coefficient based on the summation of the direct readings on the two Y-gages,

$Y_{GR'}$ is the X-force coefficient based on the summation of the direct readings on the two X-gages

m' is the mass coefficient based on the total weight or displacement of the model,

m_Y' is the mass coefficient based on the portion of the model weight not sensed by the Y-gages, and

m_X' is the mass coefficient based on the portion of the model weight not sensed by the X-gages

To enable independent analysis, the numerical values of the hydrodynamic coefficients X', Y', and N' obtained by the foregoing reduction process are presented in the appendixes both as tables of individual data points and as cross-curves showing the functional relationship between these hydrodynamic coefficients and the kinematic variables r', β, δ_R. Appendix A contains the data obtained from the rotating-arm tests for the 20-knot and 10-knot conditions and Appendix B contains the data obtained from the straightline tests at the same two conditions. Included in Appendix B are the results of propulsion tests of the MARINER model conducted at approximately standard conditions and the results of open-water tests of the model propeller used in all of the experiments.

In the body of the report, faired curves of X', Y', and N' and associated data points, separately expressed as functions of β, r', and δ_R, are presented for the so-called reference conditions. These curves are plotted on a scale which is intended to be large enough to permit quantitative determination of stability and control derivatives; to accentuate the degree of scatter among data points; and to indicate trends such as the existence of nonlinearities. In addition, the free motions (roll angles and pitch angles) recorded during the tests are presented as faired curves in which the angles are separately expressed as functions of β, r', and δ_R. The stability and control derivatives determined from the reference curves, and in some cases from the cross-curves in the appendixes, are presented in the form of tables which compare the numerical values obtained either by different test techniques or by different laboratories.

DISCUSSION OF DATA

As mentioned in the Introduction, the subject investigation is concerned primarily with experimental techniques. Accordingly, in the discussion that follows, the emphasis is placed on accuracy, repeatability, trends, and other factors pertinent to the technique, rather than to the significance of the data in regard to quality of design and expected performance of the specific ship. The

data obtained from each of the two types of captive-model tests are first discussed independently and then the two techniques are compared on basis of numerical values obtained for certain stability and control derivatives.

ROTATING-ARM TESTS

Typical data obtained from the rotating-arm tests are shown by the reference curves presented in Figures 3, 4, and 5 for the 20-knot condition and in Figures 6 and 7 for the 10-knot condition.

Figure 3 shows the variation of the hydrodynamic coefficients X', Y', and N' with the nondimensional angular velocity component r' for the 20-knot condition, as derived from Test Group 3R (Table 2). In general, the data points for each of these hydrodynamic coefficients follow a smooth faired curve over the entire range investigated. The small amount of scatter shown around r' = 0.2045 in each case, is a measure of repeatability since three of the four data points were obtained from other groups of tests. Two of these groups of tests involved changes in either yaw-angle setting or rudder-angle setting. It is very difficult to restore the model to identically the same initial settings, especially where these settings are zero, after such changes have been made. It is considered, therefore, that the small amount of scatter shown constitutes good repeatability. It is interesting to note that the Y'-curve is nearly linear up to an r' of about 0.4 and that the N'-curve is nearly linear up to an r' of about 0.3. Characteristically, the X' curve is nonlinear, but the change in X', with constant propeller rpm, is very small over a wide range of r'. The range of r' covered in the experiments is in excess of that attained by the full-scale ship[2] (r' of about 0.6).

Figure 4 shows the variation of the hydrodynamic coefficients X', Y', and N' with β, as derived from Test Group 1R. The points for this variation also fall on reasonably faired curves and exhibit very little scatter. The amount of scatter shown at $\beta = 0$ is, of course, equivalent to that shown in Figure 3 at r' = 0.2045. The Y'-curve is nearly linear up to a β of about 7 degrees. However, the N'-curve , as well as the X'-curve, tends to be nonlinear over the entire range of β-values. It should be understood, however, that the range of β - values covered by the experiments is greatly in excess of the maximum steady β that can be attained by the full-scale ship which was shown to be about 13 degrees[2].

Figure 5 shows the variation of the hydrodynamic coefficients X', Y', and N' with δ_R, as derived from Test, Group 2R. In addition to the scatter about $\delta_R = 0$, which is equivalent to that shown about r' = 0.2045 and $\beta = 0$ in Figures 3 and 4, respectively, there is scatter in the Y'- and N'- data over a range of δ_R from 0 to 15 degrees. It is believed that this could be due, for most part, to lost motion between the rudderstock and the angle sensor located in the actuator. An attempt to overcome this type of lost motion was made by installing a spring in the actuator system prior to conducting the experiments. Nevertheless, the data indicate that there may have been lost motion amounting to as much as 1

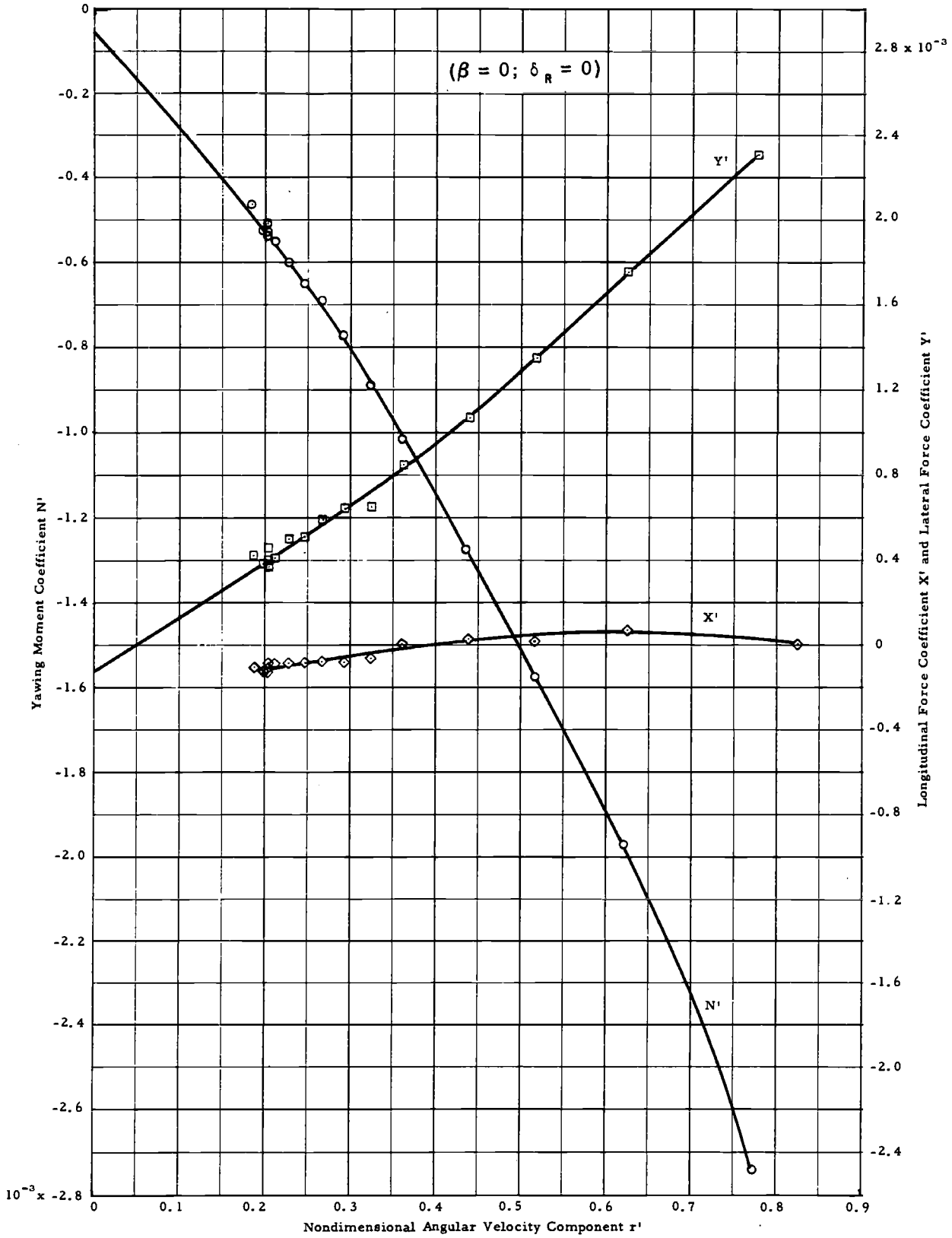

Figure 3 - Typical Data from Rotating-Arm Tests Showing Variation of Hydrodynamic Coefficients X', Y' and N' with Nondimensional Angular Velocity Component r' (20-Knot Condition)

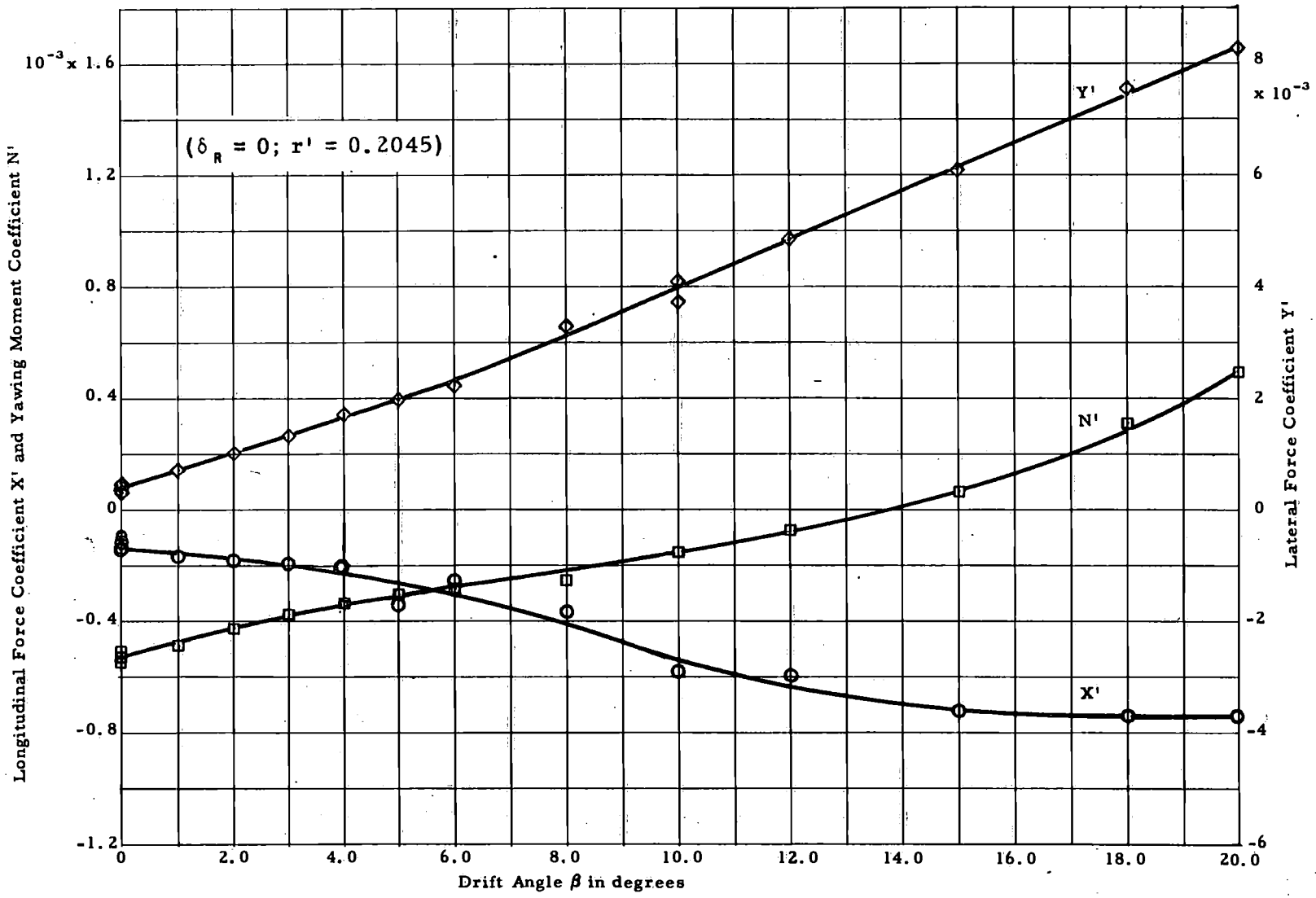

Figure 4 - Typical Data from Rotating-Arm Tests Showing Variation of Hydrodynamic Coefficients X', Y', and N' with Drift Angle β (20-Knot Condition)

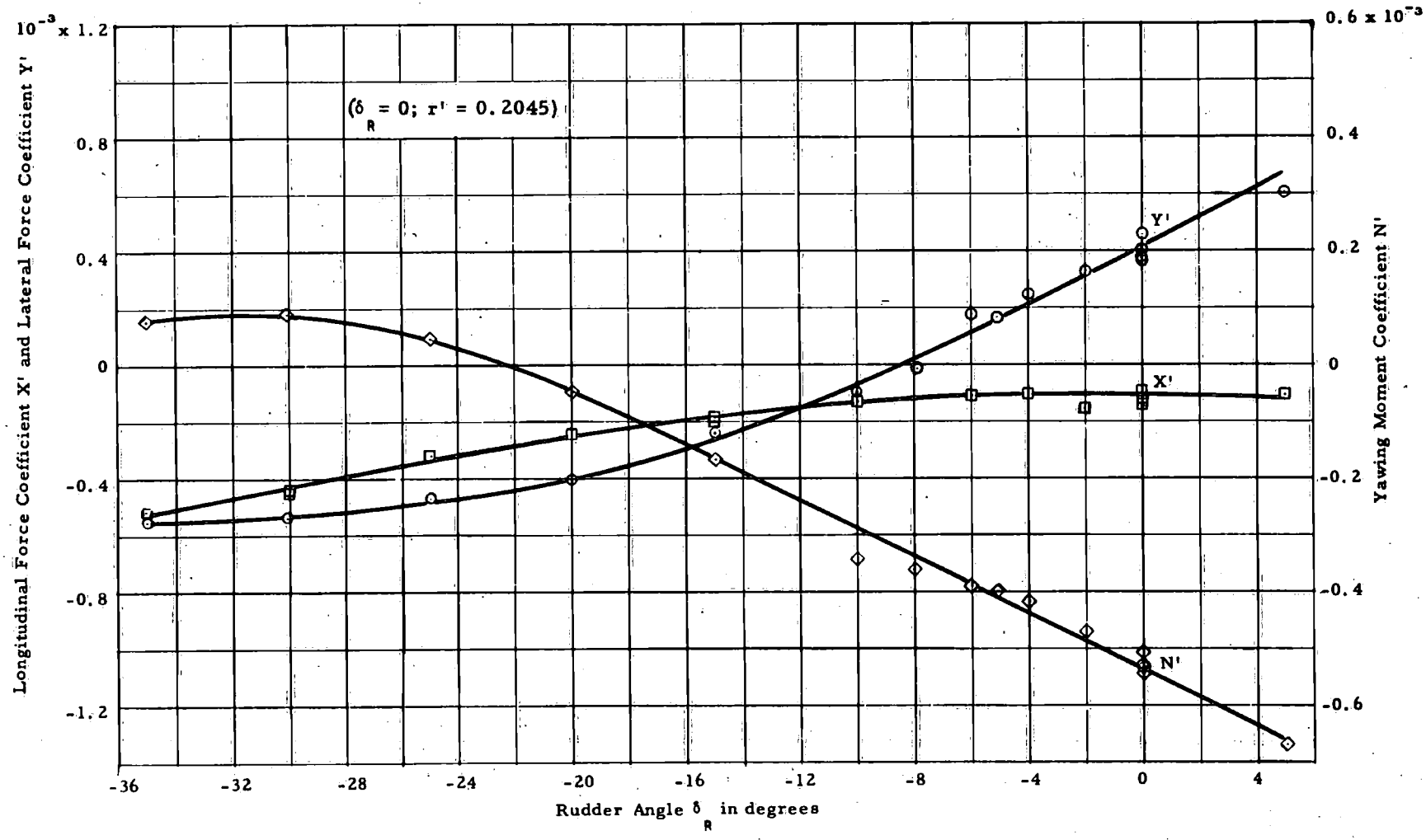

Figure 5 - Typical Data from Rotating-Arm Tests Showing Variation of Hydrodynamic Coefficients X', Y', and N' with Rudder Angle δ_R (20-Knot Condition)

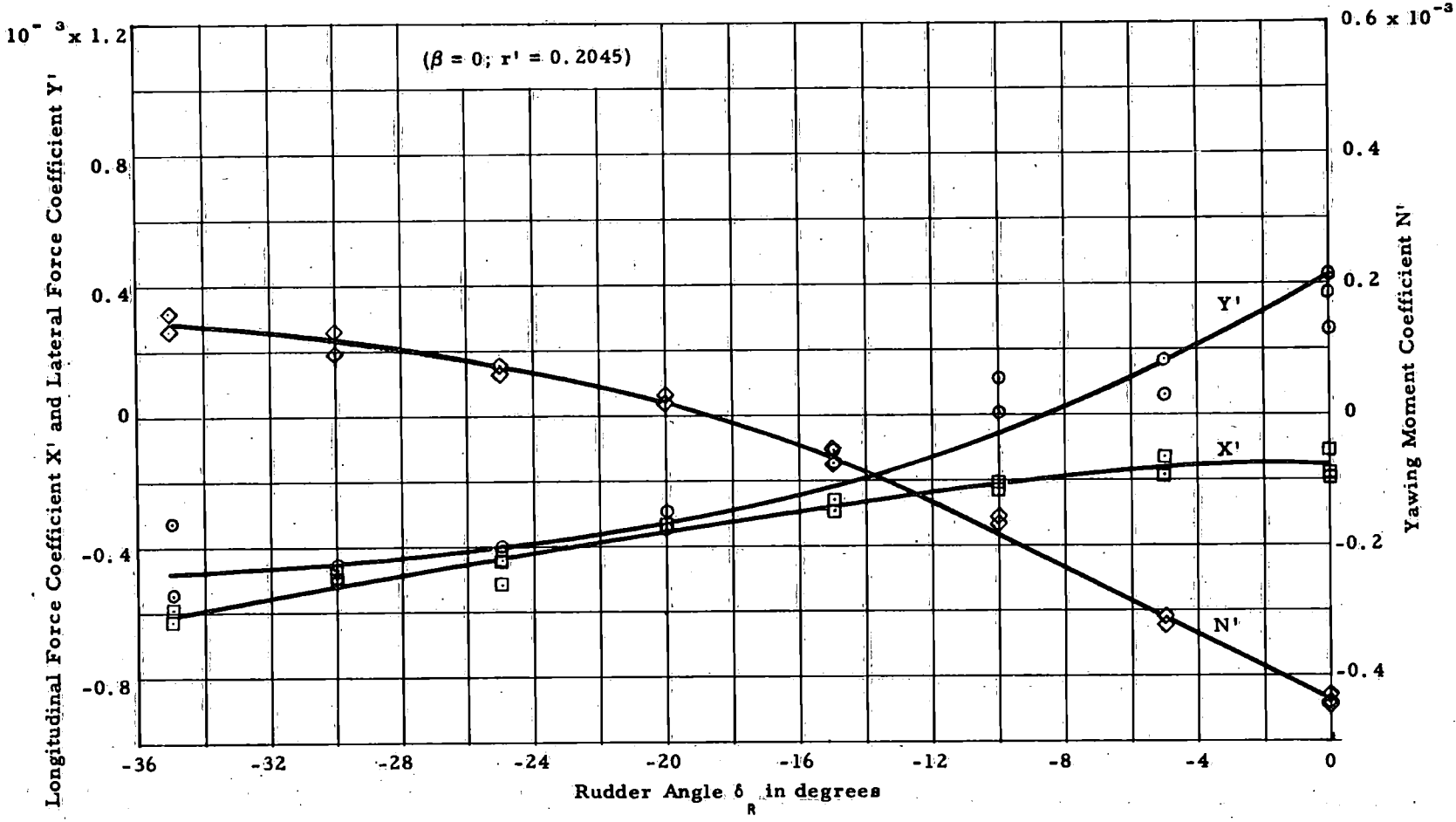

Figure 6 - Typical Data from Rotating-Arm Tests Showing Variation of Hydrodynamic Coefficients X', Y', and N' with Rudder Angle δ_R (10-Knot Condition)

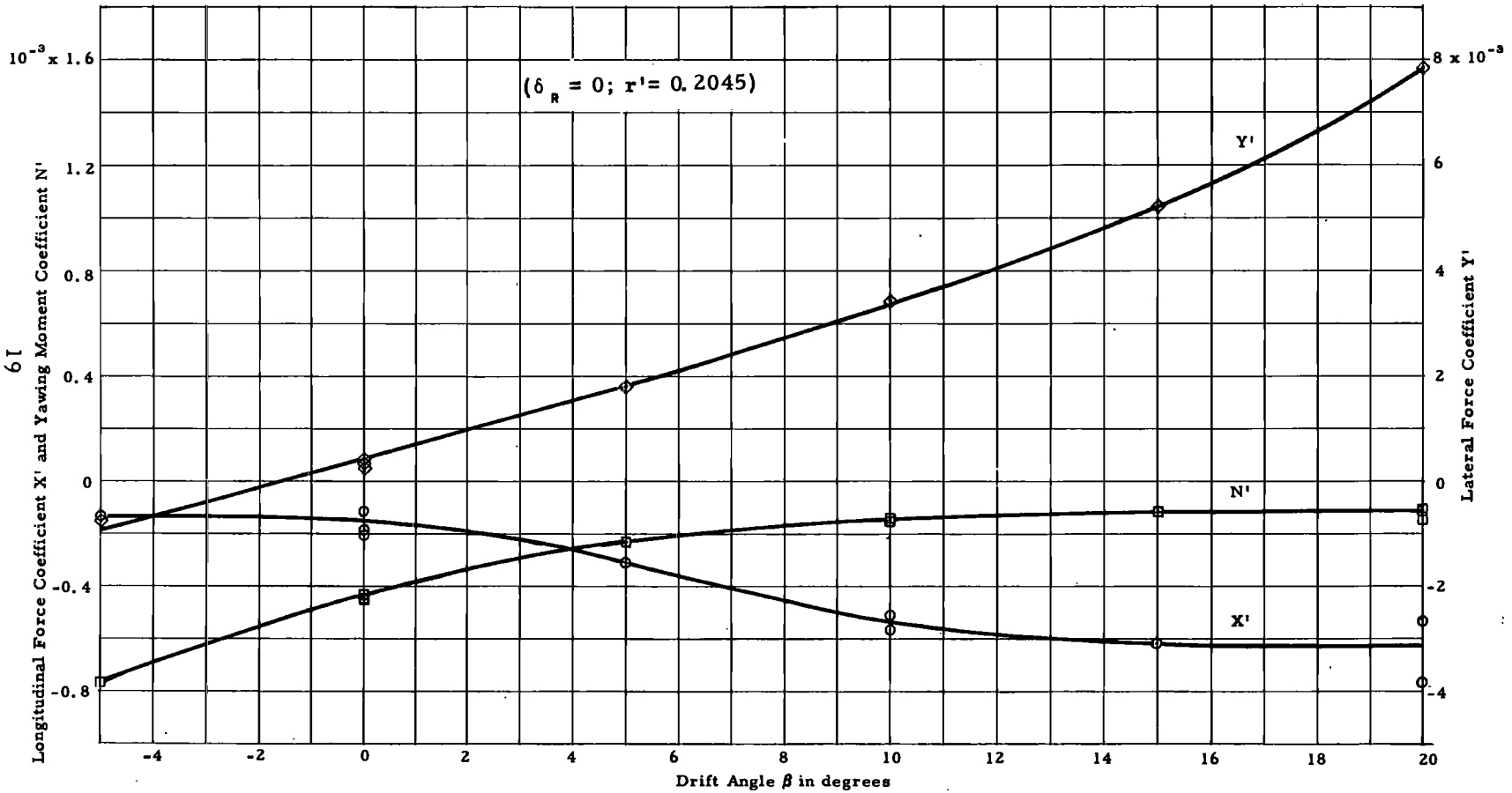

Figure 7 - Typical Data from Rotating-Arm Tests Showing Variation of Hydrodynamic Coefficients X', Y', and N' with Drift Angle β (10-Knot Condition)

degree. Since the experiments were conducted, the Model Basin has developed a new device that accurately senses the angle at the rudderstock, which should correct this difficulty in future experiments of this kind. The figure shows that the Y'- and N'-curves are nearly linear over a range of δ_R values from 0 to at least 12 degrees.

As mentioned previously, the rotating-arm tests conducted for the 10-knot condition were comparatively incomplete. However, some observations can be made on basis of the data presented in Figures 6 and 7. The variation of the hydrodynamic coefficients X', Y', and N' with δ_R is shown by Figure 6. In comparison with Figure 5, there appears to be considerably more scatter for the 10-knot condition than for the 20-knot condition. This would normally be expected since the forces being measured with the same instrumentation for the 10-knot condition are about one-fourth the magnitude of the comparable forces for the 20-knot condition. In spite of this, however, there appears to be very little scatter in the data for the β-variation shown in Figure 7. The scatter in Figure 6 may be explained, at least in part, by the erratic flow conditions in the vicinity of the rudder resulting from the relatively low Reynolds numbers for the 10-knot condition.

All in all, the data from the rotating-arm tests appear to be reasonably accurate, consistent, and repeatable on a day to day basis. Some improvement can be expected in the future when towing apparatus and other equipment which is specifically designed for captive-model testing of surface-ship models on the Rotating Arm Facility becomes available.

STRAIGHTLINE TESTS

Typical data obtained from the straightline tests are shown by Figures 8 and 9 for the 20-knot condition and by Figures 10 and 11 for the 10-knot condition. As mentioned previously, only the δ_R-variation (Group 1S in Table 3) can be considered truly as a reference test since it involves changing only one parameter (δ_R) while the other (β) remains unchanged throughout the group of runs.

Figure 9 shows that, for the 20-knot condition, the data from the reference test define a faired curve with very little scatter. The small spread between the pairs of data points at any given rudder setting is due to the fact that the data are obtained from two separate sets of runs. To this extent, this spread is indicative of the repeatability of the data. Figure 11 shows equally good results for the 10-knot condition insofar as scatter of data is concerned. Figures 9 and 11 both show that the Y'- and N'-curves are nearly linear over a range of δ_R values of from 0 to at least 12 degrees, as was the case for the rotating-arm tests.

The data points for the β-variation (Figures 8 and 10) also appear to fall on smooth faired curves with very little scatter. It would have been desirable, however, if the β-variation had been performed as a reference test with β varied in 1 or 2-degree increments between 0 and 10 degrees. This would have permitted a more precise delineation of the Y'- and N'-curves which, in turn,

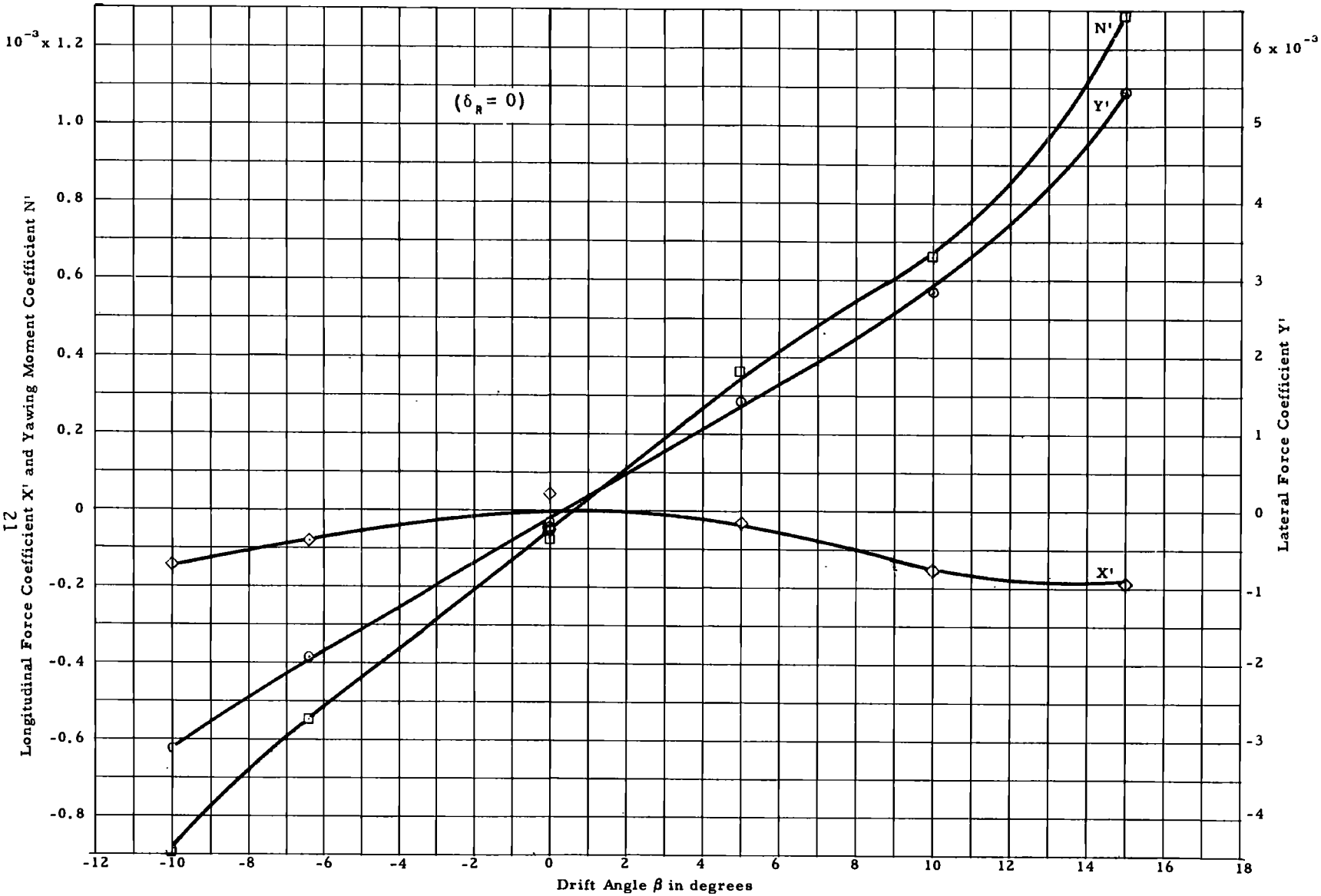

Figure 8 - Typical Data from Straightline Tests Showing Variation of Hydrodynamic Coefficients X', Y', and N' with Drift Angle β (20-Knot Condition)

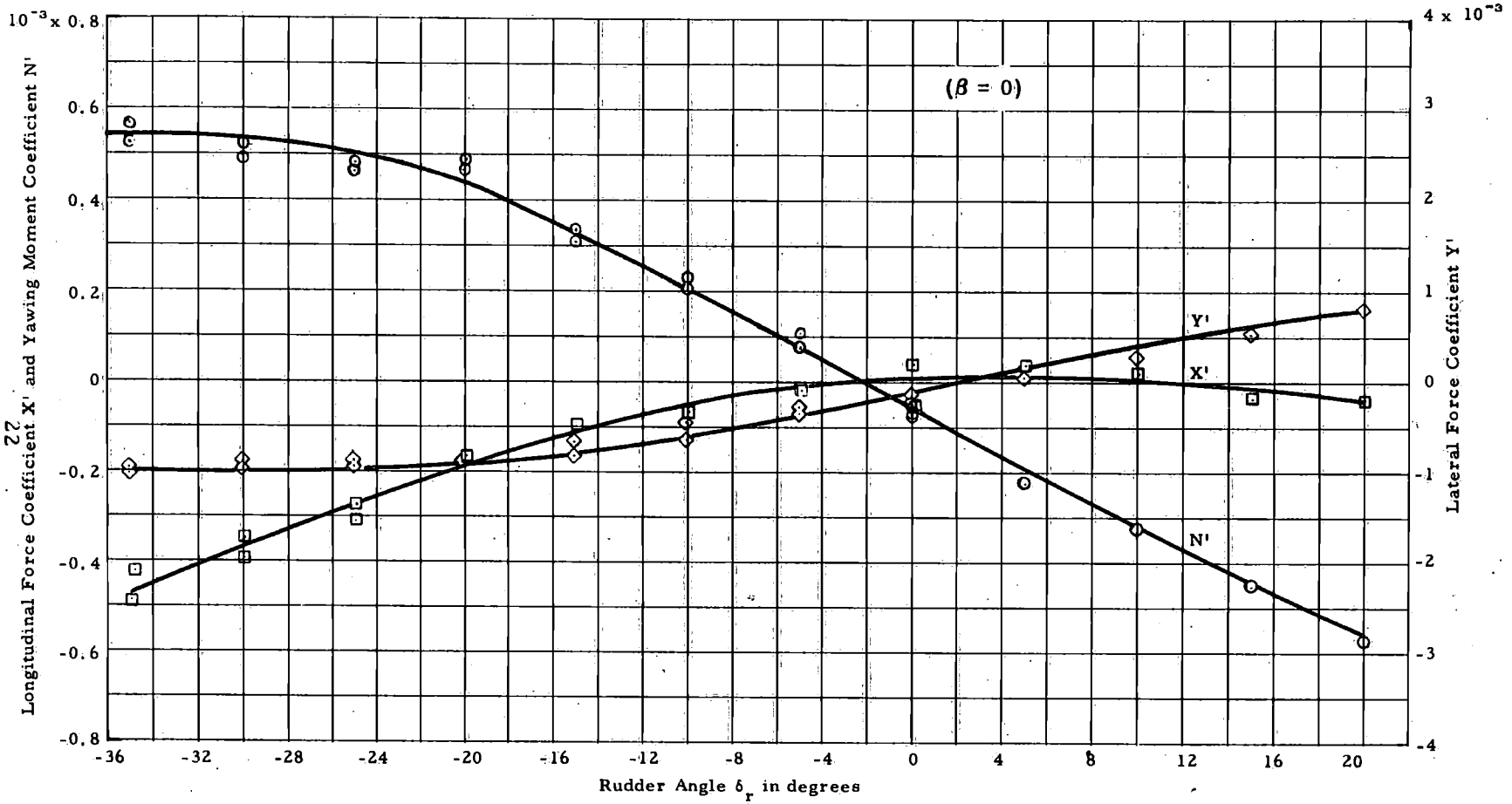

Figure 9 - Typical Data from Straightline Tests Showing Variation of Hydrodynamic Coefficients X', Y', and N' with Rudder Angle δ_R (20-Knot Condition)

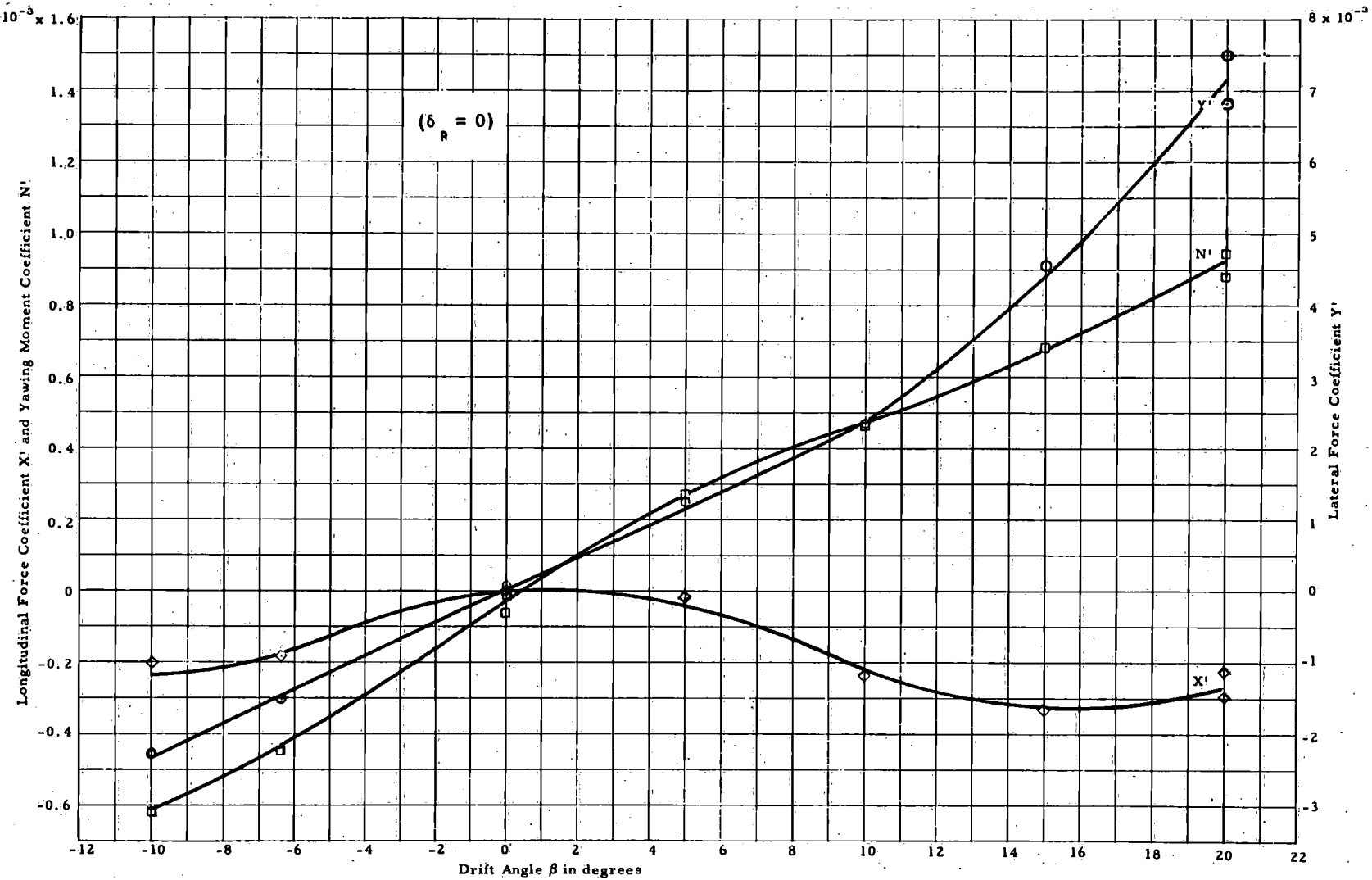

Figure 10 - Typical Data from Straightline Tests Showing Variation of Hydrodynamic Coefficients X', Y', and N' with Drift Angle β (10-Knot Condition)

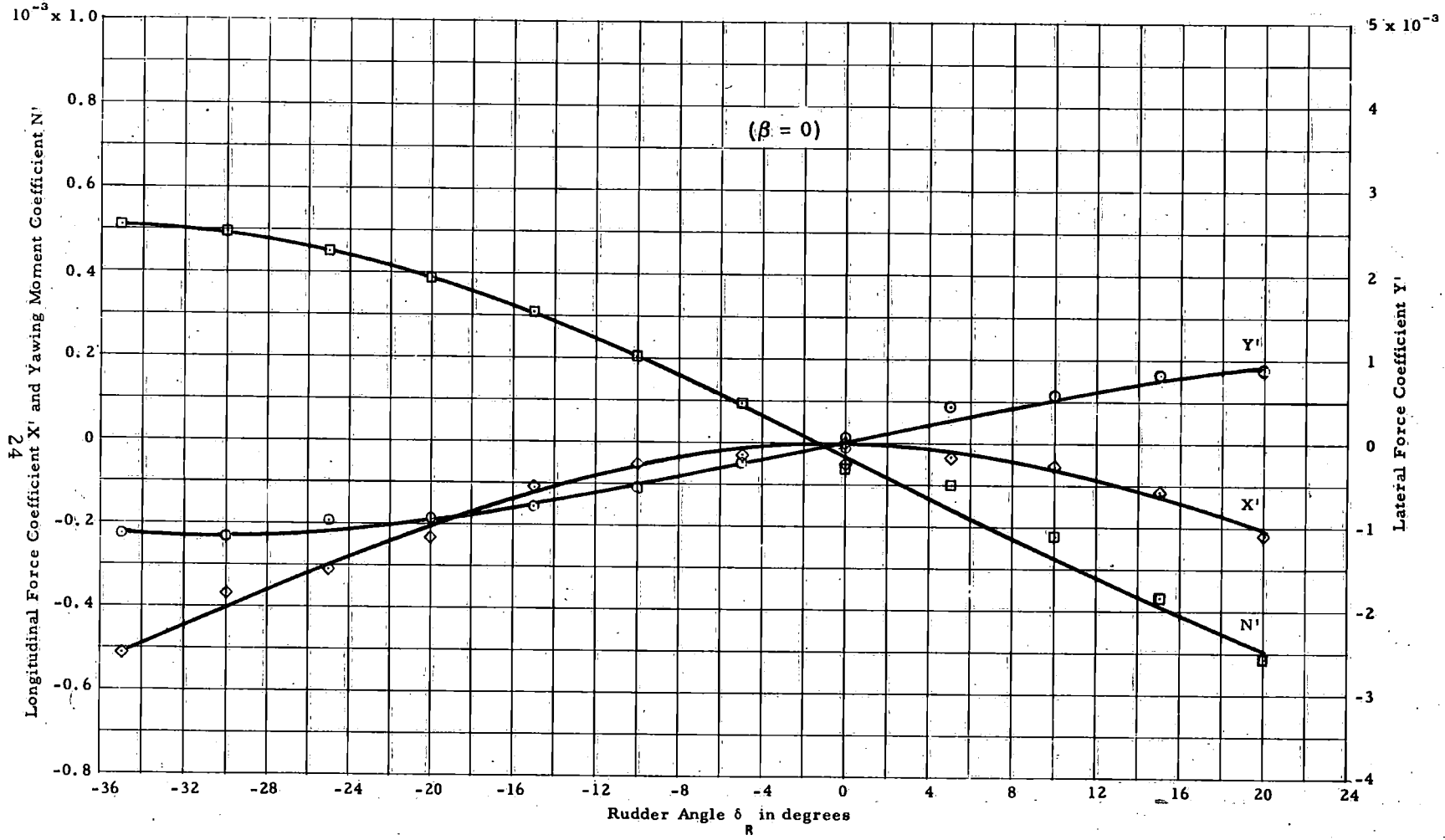

Figure 11 - Typical Data from Straightline Tests Showing Variation of Hydrodynamic Coefficients X', Y', and N' with Rudder Angle δ_R (10-Knot Condition)

would have enabled a more accurate determination of the static derivatives Y_v' and N_v'.

In spite of the way that the tests for the β-variation were conducted, the data from the straightline tests appear to be reasonably accurate, consistent, and repeatable.

COMPARISON OF THE TWO TECHNIQUES

The data obtained from the rotating-arm and straightline tests are compared in Table 4 on the basis of stability and control derivatives. The most direct comparison that can be made between the two techniques is with the derivatives Y_{δ_R} and N_{δ_R}. This is because, in the subject experiments, r' had very little influence on these two derivatives. For example, the derivatives read off the Y' and N' versus δ_R-curves for the cases of R' = 0.2045 and R' = 0.2930 had essentially the same values. Consequently, it was assumed that no extrapolation to r' = 0 was required. It may be seen from Table 4 that the values of Y_{δ_R}' and N_{δ_R}' obtained from the rotating-arm tests agree with the corresponding values from the straightline tests within 4 percent for the 20-knot condition; the values from the two techniques agree almost exactly for the 10-knot condition. This demonstrates that if the same model, the same instrumentation, and the same test procedures are used, it is possible to obtain essentially the same values for the two rudder derivatives from tests in the two facilities. It should be noted that, within the accuracy of the experiments, the results of both the rotating-arm tests and straightline tests indicate that the values for both Y_{δ_R}' and N_{δ_R}' do not change in going from the 20-knot to the 10-knot condition.

The precise agreement shown by Table 4 in the values of Y_v' and N_v' obtained by the two techniques must be considered as fortuitous. The values listed for the straightline tests are considered to be reliable since they are obtained by means of a direct process. On the other hand, the values listed for the rotating-arm tests were obtained by extrapolating the appropriate cross-curves given in Appendix A to the case of r' = 0. As mentioned previously, the reference value r' = 0.2045 was selected with the hope that the slopes of the Y'- and N' versus β-curves at β= 0 would approach those for the straightline case. This turned out on the subject tests to be a reasonably good assumption for Y_v', but not for N_v'. For example, the values of Y_v' and N_v' read from the reference curves (r' = 0.2045) for the 20-knot condition are 17.48×10^{-3} and 3.065×10^{-3} compared, respectively, with 16.90×10^{-3} and 4.469×10^{-3} shown for the straightline case in Table 4. Thus it appears that there is a fairly strong coupling effect of r' on β as far as the yawing moment coefficient is concerned even at small values of r' and β. It should be noted from Table 4 that the values for the derivatives Y_v' and N_v' for the 20-knot condition differ considerably from those for the 10-knot condition.

TABLE 4

Stability and Control Derivatives Determined From Rotating-Arm and Straightline Tests

(Values must be multiplied by 10^{-3})

Derivative	20-Knot Condition		10-Knot Condition		20-Knot Condition Without Propeller
	Rotating-Arm	Straightline	Rotating-Arm	Straightline	Rotating-Arm
Y_v'	-16.90	-16.90	-	-13.29	-
N_v'	-4.47	-4.47	-	-3.51	-
$Y_{\delta r}'$	2.87	2.98	2.861	2.87	1.47
$N_{\delta r}'$	-1.38	-1.43	-1.374	-1.38	-0.71
Y_r'	2.62	-	-	-	-
N_r'	-2.30	-	-	-	-

NOTE: All values except those for the case without propellers correspond to the point of propulsion for the full-scale ship which is taken to be at a propeller advance coefficient $J = \frac{U}{nD} = 0.979$. All derivatives listed for the Rotating-Arm except $Y_{\delta r}'$ and $N_{\delta r}'$ were obtained by extrapolating the data to a case of $r' = 0$.

The values given in Table 4 for the rotary derivatives Y_r' and N_r' are considered to be reliable since they are obtained directly from the results of a properly conducted rotating-arm reference test. Since rotary derivatives cannot be obtained from a simple straightline test , it is planned for the future to conduct tests in the straightline basin with a planar motion mechanism using the same model and measuring equipment. This should provide rotary derivatives from an alternative technique which can be compared with those in Table 4.

For the case of $\beta = r' = \delta_R = 0$, the lateral force and yawing moment on a single-screw ship are not zero but usually have some finite value. These are usually denoted in nondimensional form as the coefficients Y_*' and N_*'. The effects of these coefficients are manifested on the actual ship by differences between the steady-turning diameters obtained from right and left turns conducted at equal rudder angles. Furthermore, the rudder setting required for equilibrium straightline flight (neutral angle) is some value other than zero. It is extremely difficult to obtain reliable numerical values for these coefficients from model tests without resorting to special procedures.

Among the two techniques, the straightline test offers the best possibilities for accurately determining Y_*' and N_*' since, at least in the ideal sense, it is possible to set the model at a condition of $\beta = r' = \delta_R = 0$. In practice, however, due to problems in alignment and asymmetries in the model itself, it is difficult to separate out the effect due to the propeller alone. It was intended to conduct a special group of straightline tests using first a right-hand propeller, then a dummy hub, and then a left-hand propeller. This would have provided data which could be used to directly determine the desired value of Y_*' and N_*' since it would eliminate the effects of uncertainties in settings of β and δ_R as well as the effects of other asymmetries in the model or towing system. Unfortunately, these tests were not conducted due to limitations in time. Consequently, the values of Y_*' and N_*' shown, for example, in Figure 8 are considered to be neither representative of the full scale nor even consistent in sign with each other.

It is even more difficult to obtain accurate values of Y_*' and N_*' from rotating-arm tests since an extrapolation on r' is required to obtain a case of $\beta = r' = \delta_R = 0$. One technique that has been suggested is to rotate the model 180 degrees about the reference point to obtain a range of negative values of r' so that an interpolation, rather than an extrapolation, could be made to the case of $\beta = r' = \delta_R = 0$. This procedure is not considered to be practical for two reasons: first, it is difficult to preserve the initial alignment at the largest radius after swinging the model around by 180 degrees and, secondly, there is no guarantee that Y' and N' will be linear between the plus and minus values of r' corresponding to the largest radius.

The previous discussion is concerned primarily with an evaluation of the two different techniques from the standpoint of determining derivatives for linearized equations of motion. It is apparent that, between these two techniques, the straightline test is the more accurate means for determining the derivatives Y_v', N_v', Y_{δ_R}' and N_{δ_R}' and the rotating arm test is required for determining Y_r' and N_r'. The straightline test is the more direct procedure for determining nonlinearities caused solely by β and δ_R variations. The rotating arm is the more direct procedure for determining nonlinearities caused solely by the r' variation. For determining coupling effects, the two techniques complement each other. The straightline test is the more direct procedure for determining Y_*' and N_*' for single-screw ships, but even here a special technique must be employed to obtain reliable results.

The separate effects of the kinematic variables β, r', and δ_R on the free motions of the ship are shown by Figures 12, 13, and 14. In all cases, the change in pitch angle θ is small, amounting to at most 0.6 degree at the 20-knot condition. The roll angle variation with r' and δ_R is also small. However, the variation with β is significantly larger, amounting to as much as -6.0 degrees at β = 13 degrees for the 20-knot condition. However, this value of β is associated with the tightest turn that the ship can make, and the speed in the turn will be considerably less than the approach speed. Consequently, the largest roll angle that would occur in the real case would probably be no more than -3.0 degrees.

COMPARISON WITH DATA OBTAINED BY OTHER ORGANIZATIONS

Reference 3 summarizes the status and results of the ITTC "Standard Captive-Model Tests" conducted by the various member organizations and reported prior to May 1966. Included are detailed comparisons made both on the basis of stability and control derivatives and on the basis of faired curves showing the variations of the hydrodynamic coefficients X', Y', and N' with the kinematic variables β, r', and δ_R. Such a comparison and the attendant implications are considered to be beyond the scope of this report. Nevertheless, it is of interest to compare those stability and control derivatives obtained in the subject investigation with corresponding derivatives obtained by other facilities and techniques. Accordingly, the pertinent derivatives are compared in Table 5. In all cases, the derivatives correspond to the standard condition closest to the 20-knot condition that was investigated by the particular organization.

It may be seen from Table 5 that, although the values produced by the David Taylor Model Basin on the two different facilities are in close agreement, there is a wide disparity between these values and the corresponding values produced by the other organizations. Some of these differences can be attributed to a variety of factors noted in Reference 3 such as the effects of: model size, basin size, the type of towing arrangement used (for example whether or not the model was free to trim), omission of appendages such as bilge keels, operating

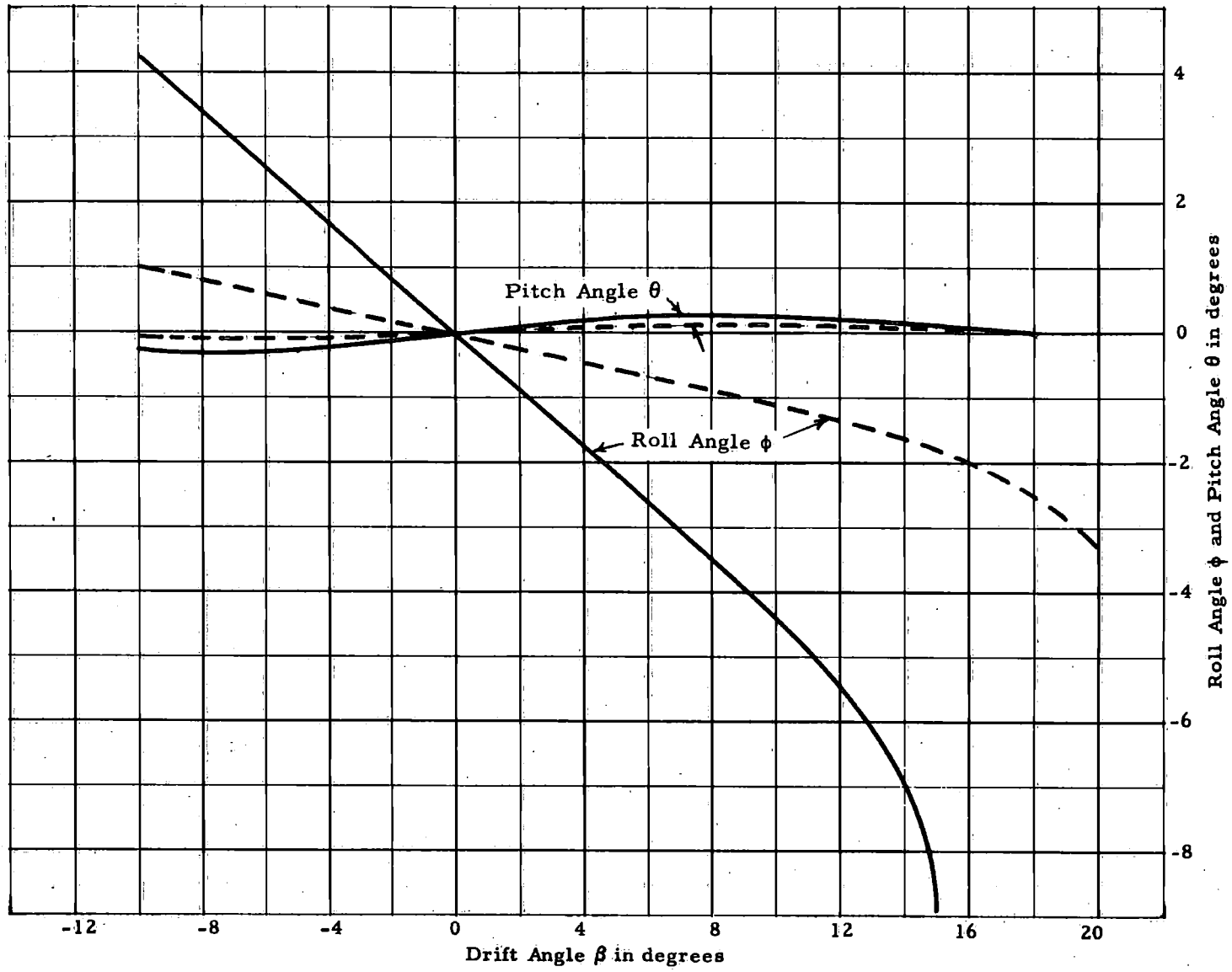

Figure 12 - Roll Angle ϕ and Pitch Angle θ as a Function of Drift Angle β
(Solid line denotes 20-knot condition; broken line denotes 10-knot condition)

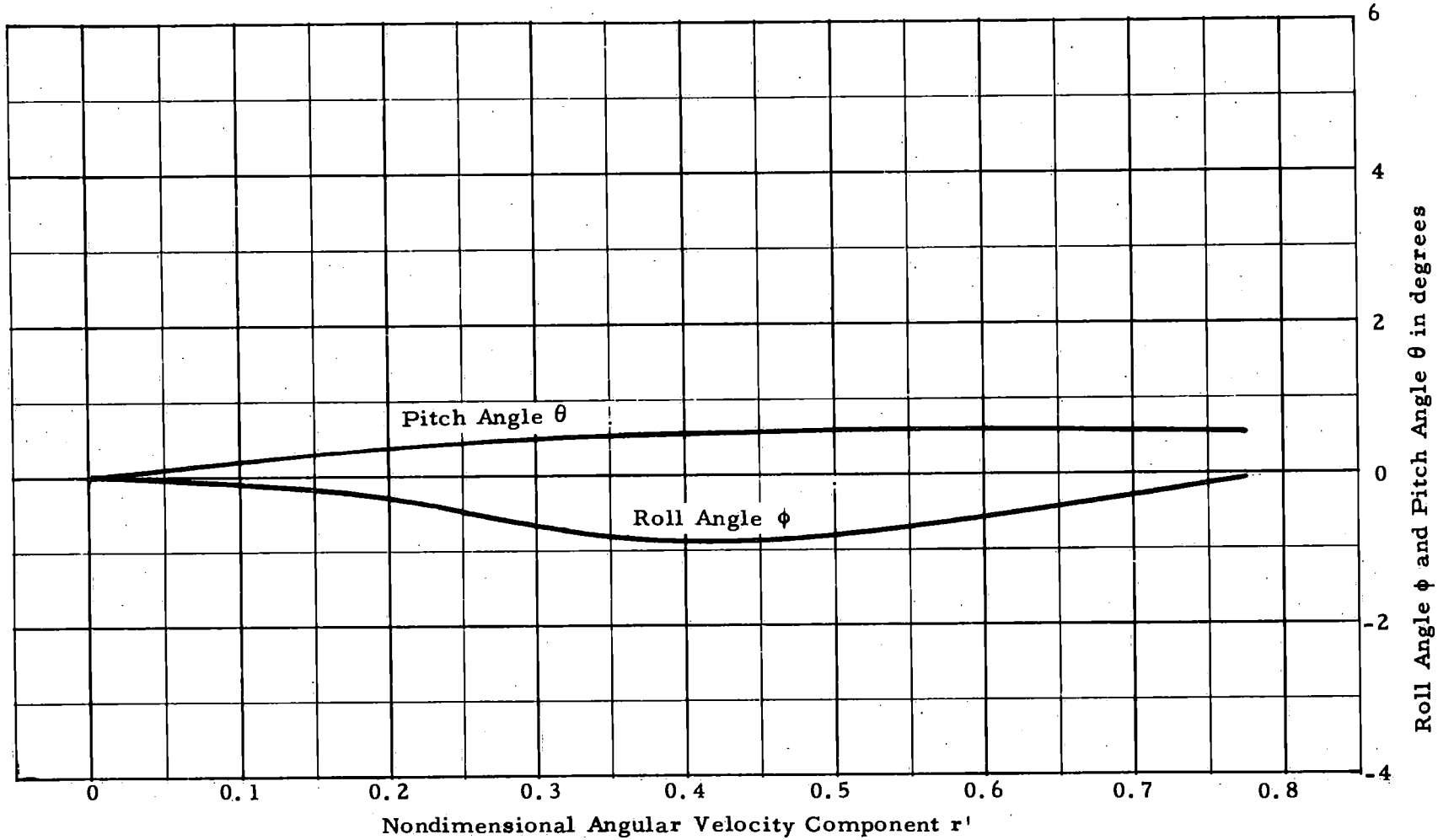

Figure 13 - Roll Angle ϕ and Pitch Angle θ as a Function of Angular Velocity r'
(Solid line denotes 20-knot condition; broken line denotes 10-knot condition)

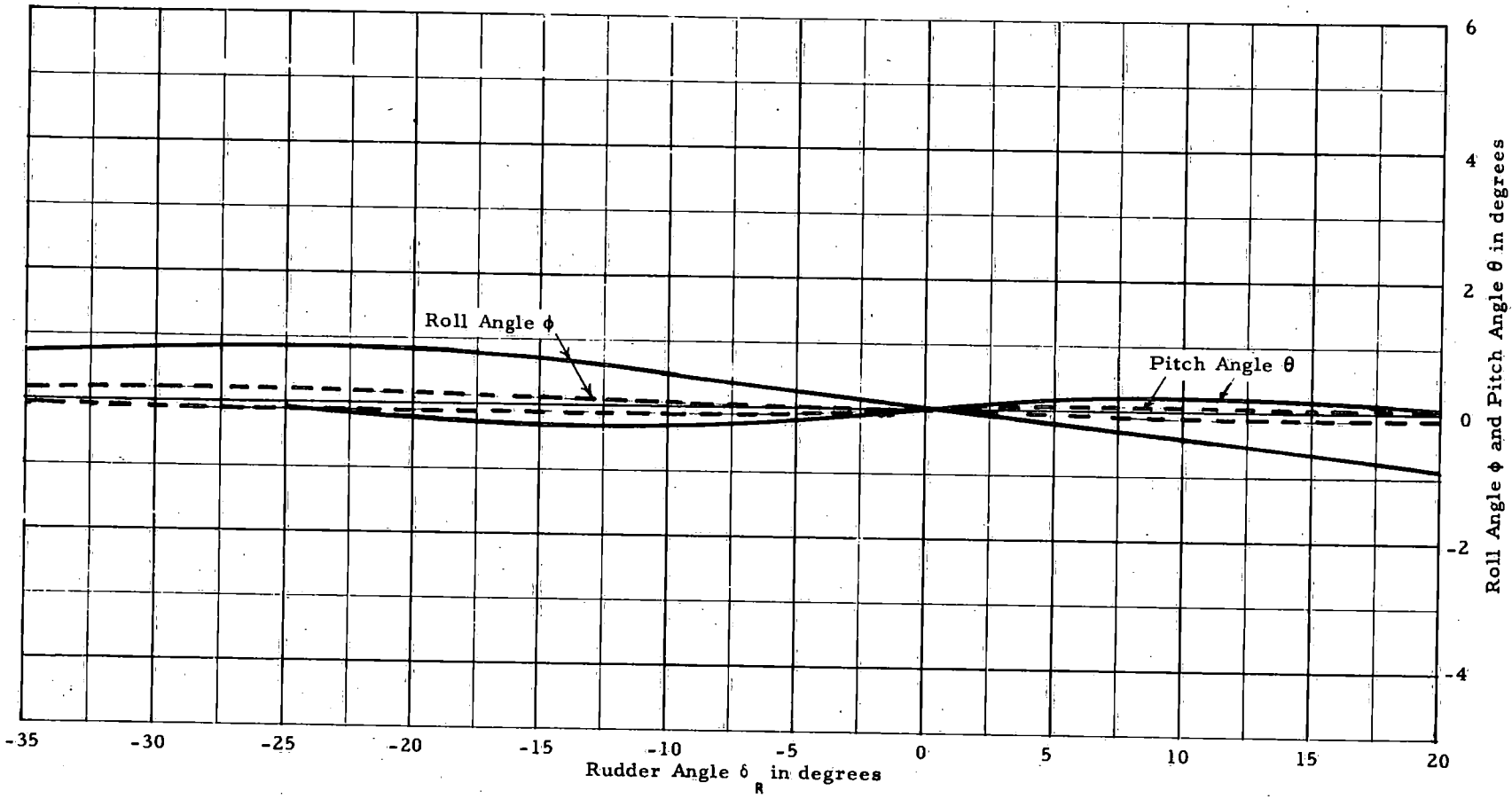

Figure 14 - Roll Angle ϕ and Pitch Angle θ as a Function of Rudder Angle δ_R
(Solid line denotes 20-knot condition; broken line denotes 10-knot condition)

TABLE 5

Comparison of Hydrodynamic Derivatives with Those Obtained by Other Organizations

(Values listed are for the standard condition closest to the 20-knot condition. The values must be multiplied by 10^{-3})

Organization	Type of Test	Y_v'	N_v'	Y_{δ_R}'	N_{δ_R}'	Y_r'	N_r'
David Taylor Model Basin, USA	Straightline	-16.90	-4.47	2.98	-1.43		
	Rotating-Arm	-16.90	-4.47	2.87	-1.38	2.62	-2.30
University of California, USA	Straightline	-11.80	-3.80				
	Planar-Motion Mechanism	-13.30	-3.80			2.60	-2.10
Hydro- and Aero-dynamics Laboratory, Denmark	Straightline	-11.60	-2.91	2.78	-1.33		
	Planar-Motion Mechanism					2.72	-1.91
Techno-logical University Delft, Holland	Planar-Motion Mechanism	-10.10	-3.49	2.32	-1.10	2.90	-2.00
Nagasaki Technical Institute	Straightline	-12.41	-4.58				

NOTE: For further particulars such as model size, basin dimensions, towing arrangement, appendages, etc. see Reference 4.

at model instead of ship point of propulsion, etc. Unfortunately, the resolution of these differences will have to remain for some future time when sufficient information is available to properly assess how the foregoing factors affect the numerical values of the stability and control derivatives.

CONCLUSIONS

On basis of rotating-arm and straightline experiments with a 22-foot long standard model (MARINER Type Ship) conducted at the David Taylor Model Basin for the ITTC Maneuverability Committee's Cooperative Program, the following conclusions are drawn:

1. If the model, instrumentation, test procedures, initial test conditions, and approach speed are kept the same, it is possible to obtain the same numerical values for the individual derivatives Y_v', N_v', Y_{δ_R}', and N_{δ_R}' in the Rotating Arm Facility as in the Straightline Basin Facility.

2. Among the two test techniques investigated, the straightline type of test is an inherently more direct and accurate method for determining the static stability and control derivatives Y_v', N_v', Y_{δ_R}', and N_{δ_R}', and the nonlinearities in the force and moment coefficients Y' and N' caused solely by variations in either β or δ_R.

3. Among the two test techniques investigated, the rotating-arm type of test is an inherently accurate technique for determining the rotary derivatives Y_r' and N_r', and the nonlinearities in Y' and N' caused solely by the r' variation. The rotary derivatives cannot be obtained by a simple straightline test, but require a planar motion mechanism or other equivalent device.

4. The two techniques complement each other when it comes to determining coupling effects in the hydrodynamic coefficients.

5. For single-screw ships, a special technique utilizing straightline tests is required to accurately determine the coefficients Y_*' and N_*' which result from an interation between the propeller and stern of the ship while on straight course.

6. In going from the 20-knot to the 10-knot condition, the values of the control derivatives Y_{δ_R}' and N_{δ_R}' do not change significantly but there is a substantial change in the values of the static stability derivatives Y_v' and N_v'. Sufficient data were not obtained for the 10-knot condition to determine whether the values of the rotary derivatives Y_r' and N_r' change significantly with approach speed.

ACKNOWLEDGMENTS

The author is grateful to those members of the Stability and Control Division of the David Taylor Model Basin who contributed to the investigation described by this report. Particular thanks are due to Mr. Samuel H. Brooks who was responsible for the adaptation of the test equipment and the preparation of the model for tests; to Mr. Erich H. Dittrich who was responsible for conducting the tests in the Rotating Arm and Straightline Basin Facilities; and to Mr. Nan King who assisted in the reduction and analysis of the data contained in this report.

REFERENCES

1. "Maneuverability Committee Report," Proceedings of the Tenth International Towing Tank Conference, Volume 1 (September 1963).

2. Morse, R. V. and Price, D., "Maneuvering Characteristics of the MARINER Type Ship (USS COMPASS ISLAND) in Calm Seas," Sperry Gyroscope Publication G7-2233-1019 prepared for David Taylor Model Basin under Contract Nonr 3061(00) (December 1961).

3. "Maneuverability Committee Report, Appendix 1, "Proceedings of the Eleventh International Towing Tank Conference (October 1966).

4. "Maneuverability Committee Report, Appendix 2," Proceedings of the Eleventh International Towing Tank Conference (October 1966).

5. Russo, V. L. and Sullivan, E. K., "Design of the MARINER Type Ship," Transactions of the Society of Naval Architects and Marine Engineers, Volume 61 (1953).

6. Brownell, W. H., "Two New Hydromechanics Research Facilities at David Taylor Model Basin," David Taylor Model Basin Report 1690 (December 1962).

7. "Research Facilities at the David Taylor Model Basin," David Taylor Model Basin Report 1913 (October 1960).

8. Gertler, Morton, "The DTMB Planar-Motion-Mechanism System," Proceedings of Symposium on Towing Tank Facilities, Instrumentation and Measuring Techniques, Zagreb, Yugoslavia (September 1959).

APPENDIX A

HYDRODYNAMIC DATA OBTAINED FROM ROTATING-ARM TESTS

(Tables 6 through 9 and Figures 15 through 20)

TABLE 6

Data from Rotating-Arm Tests for 20-Knot Condition

$$\left(F = \frac{U}{\sqrt{gL}} = 0.259,\ J = \frac{U}{nD} = 0.979\right)$$

(Values for Coefficients X', Y', and N' must be multiplied by 10^{-3})

r'	β degrees	δ_R degrees	X'	Y'	N'
0.2045	0.0	0.0	-0.135	0.379	-0.530
	1.0		-0.169	0.706	-0.487
	2.0		-0.186	1.009	-0.427
	3.0		-0.197	1.325	-0.377
	4.0		-0.220	1.725	-0.335
	5.0		-0.346	1.990	-0.305
	6.0		-0.259	2.253	-0.282
	8.0		-0.368	3.306	-0.251
	10.0		-0.582	4.120	-0.149
	12.0		-0.599	4.896	-0.070
	15.0		-0.724	6.101	0.069
	18.0		-0.742	7.599	0.314
	-5.0		-0.116	-1.057	-1.024
0.2045	0.0	0.0	-0.124	0.400	-0.507
0.2045	0.0	-5.1		0.165	-0.400
		0.0	-0.087	0.460	-0.509
		5.0	-0.101	0.603	-0.669
		-2.0	-0.157	0.334	-0.470
		-4.0	-0.101	0.250	-0.420
		-6.0	-0.101	0.180	-0.383
		-7.9		-0.016	-0.362
		-10.0		-0.093	-0.343
		-15.0		-0.240	-0.167
		-20.0		-0.407	-0.046
		-25.0		-0.468	0.049
		-30.0		-0.538	0.093
0.2045	0.0	-35.0		-0.554	0.080

TABLE 6 (Con't)

Data from Rotating-Arm Tests for 20-Knot Condition

$$\left(F = \frac{U}{\sqrt{gL}} = 0.259,\ J = \frac{U}{nD} = 0.979\right)$$

(Values for Coefficients X′, Y′, and N′ must be multiplied by 10^{-3})

r′	β degrees	δ_R degrees	X′	Y′	N′
0.1858	0.0	0.0	-0.106	0.423	-0.463
0.1982			-0.129	0.387	-0.527
0.2045			-0.129	0.371	-0.543
0.2112			-0.092	0.415	-0.551
0.2274			-0.087	0.503	-0.600
0.2462			-0.092	0.513	-0.655
0.2667			-0.083	0.593	-0.690
0.2930			-0.083	0.645	-0.778
0.3249			-0.069	0.653	-0.892
0.3616			0.0	0.858	-1.015
0.4398			0.028	1.068	-1.277
0.5164			0.016	1.357	-1.577
0.6246			0.092	1.758	-1.976
0.7757	0.0	0.0	-0.002	2.305	-2.743
0.6246	20.0	0	-1.182	13.916	-2.733
	15.0		-0.912	10.215	-2.420
	10.0		-0.661	6.990	-2.135
	5.0		-0.269	3.860	-1.884
0.6246	-5.0	0	0.232	-1.201	-2.337
0.6246	0.0	-5.0	0.175	1.463	-1.865
		-10.0	0.088	1.116	-1.739
		-15.0	0.078	0.792	-1.615
		-20.0	-0.028	0.815	-1.457
		-24.8	-0.115	0.727	-1.365
		-25.0	-0.097	0.553	-1.400
		-30.0	-0.226	0.374	-1.295
		-35.0	-0.272	0.301	-1.219
0.6246	0.0	-20.4	-0.005	0.748	-1.441

TABLE 6 (Con't)

Data from Rotating-Arm Tests for 20-Knot Condition

$$(F = \frac{U}{\sqrt{gL}} = 0.259,\ J = \frac{U}{nD} = 0.979)$$

(Values for Coefficients X', Y', and N' must be multiplied by 10^{-3})

r'	β degrees	δ_R degrees	X'	Y'	N'
0.6246	10.0	-5.0	-0.491	7.096	-1.983
		-10.0	-0.541	6.817	-1.808
		-15.0	-0.601	6.364	-1.669
		-20.3	-0.689	5.943	-1.470
		-25.0	-0.823	5.570	-1.311
		-30.0	-0.864	6.001	-1.181
		-34.9	-0.989	5.435	-1.167
		-30.0	-1.035	5.679	-1.232
0.6246	10.0	-10.0	-0.712	6.475	-1.770
0.6246	20.0	-5.0	-1.237	13.912	-2.610
		-10.0	-1.408	13.802	-2.448
		-15.0	-1.279	12.593	-2.239
		-20.0	-1.509	12.943	-2.090
		-25.0	-1.583	12.190	-1.881
		-30.0	-1.684	12.636	-1.732
		-35.0	-1.813	12.309	-1.739
0.6246	20.0	-15.0	-1.389	13.292	-2.271
0.2930	20.0	0.0	-0.709	8.952	-0.196
	15.0		-0.747	6.587	-0.434
	10.0		-0.503	4.396	-0.535
	5.0		-0.202	2.199	-0.608
	-5.0		0.092	-0.996	-1.387
	15.0		-0.742	6.618	-0.456
0.2930	20.0	0.0	-0.875	9.168	-0.171
0.2930	0.0	-5.0	-0.046	-0.007	-0.731
		-10.0	-0.074	-0.172	-0.617
		-15.0	-0.101	-0.222	-0.479
		-20.0	-0.217	-0.232	-0.302
		-25.0	-0.277	-0.329	-0.193
		-30.0	-0.410	-0.354	-0.139
0.2930	0.0	-35.0	-0.493	-0.418	-0.139

TABLE 6 (Con't)

Data from Rotating-Arm Tests for 20-Knot Condition

$$(F = \frac{U}{\sqrt{gL}} = 0.259,\ J = \frac{U}{nD} = 0.979)$$

(Values for Coefficients X', Y', and N' must be multiplied by 10^{-3})

r'	β degrees	δ_R degrees	X'	Y'	N'
0.2930	10.0	0.0	-0.083	4.482	-0.532
		-5.0	-0.475	4.114	-0.366
		-10.0	-0.503	3.813	-0.212
		-15.0	-0.609	3.596	-0.082
		-20.0	-0.743	3.368	0.049
		-25.0	-0.909	3.871	0.220
		-30.0	-0.950	3.343	0.205
		-35.0	-1.075	3.518	0.317
		-25.0	-0.872	3.654	0.195
		-10.0	-0.549	3.836	-0.232
		-30.0	-0.959	3.575	0.241
0.2930	10.0	-35.0	-1.042	3.547	0.305
0.2930	20.0	-5.0	-0.755	8.828	-0.016
		-10.0	-0.805	8.624	0.120
		-15.0	-0.842	8.317	0.298
		-20.0	-0.934	8.224	0.472
		-25.0	-1.050	7.774	0.580
		-30.0	-1.119	7.850	0.684
		-35.0	-1.257	7.605	0.703
		-25.0	-1.064	7.743	0.586
		-30.0	-1.165	7.605	0.637
		-20.0	-1.479	7.882	0.421
		0.0	-0.884	9.019	-0.186
		-35.0	-1.276	7.767	0.766
0.2930	20.0	-20.0	-0.902	8.059	0.476
0.2045	0.0	-10.0	-0.129	-0.257	-0.349
		-15.0	-0.198	-0.232	-0.168
		-20.0	-0.240	-0.459	-0.046
		-25.0	-0.318	-0.587	0.048
		-35.0	-0.516	-0.642	0.072
		-20.0	-0.249	-0.422	0.050
0.2045	0.0	-15.0	-0.189	-0.249	-0.167

TABLE 6 (Con't)

Data from Rotating-Arm Tests for 20-Knot Condition

$$\left(F = \frac{U}{\sqrt{gL}} = 0.259,\ J = \frac{U}{nD} = 0.979\right)$$

(Values for Coefficients X', Y', and N' must be multiplied by 10^{-3})

r'	β degrees	δ_R degrees	X'	Y'	N'
0.2045	10.0	0.0	-0.465	3.723	-0.141
		-5.0	-0.501	3.478	0.008
		-10.0	-0.525	3.196	0.143
		-15.0	-0.654	3.354	0.301
		-20.0	-0.741	3.113	0.444
		-25.0	-0.833	2.963	0.541
		-30.0	-0.875	2.851	0.609
		-34.9	-0.963	2.842	0.667
		-35.0	-0.967	2.688	0.678
		-5.0	-0.478	3.506	0.012
		-15.0	-0.649	3.293	0.308
0.2045	10.0	-15.0	-0.626	3.453	0.328
0.2045	20.0	0.0	-0.740	8.281	0.490
		-5.0	-0.768	8.074	0.595
		-35.0	-1.247	7.475	1.354
		-10.0	-0.768	7.923	0.747
		-15.0	-0.883	8.068	0.953
		-25.0	-1.044	7.645	1.261
		-30.0	-1.095	7.675	1.382
		-35.0	-1.187	7.728	1.442
		-20.0	-0.947	7.817	1.135
		-20.0	-0.961	7.836	1.076
		-15.0	-0.887	7.743	0.879
		-30.0	-1.155	7.715	1.324
0.2045	20.0	-35.0	-1.275	7.966	1.437

TABLE 7

Data from Rotating-Arm Tests for 10-Knot Condition

$$\left(F = \frac{U}{\sqrt{gL}} = 0.1295\ ,\ J = \frac{U}{nD} = 0.979\right)$$

(Values for Coefficients X', Y', and N' must be multiplied by 10^{-3})

r'	β deg	δ_R deg	X'	Y'	N'
0.2045	-5.0	0.0	-0.132	-0.774	-0.768
	0.0		-0.202	0.262	-0.450
	+5.0		-0.309	1.812	-0.232
	10.0		-0.508	3.452	-0.136
	15.0		-0.618	5.244	-0.111
0.2045	20.0	0.0	-0.768	7.886	-0.101
0.2045	0.0	0.0	-0.184	0.428	-0.432
		-5.0	-0.184	0.170	-0.321
		-10.0	-0.221	0.115	-0.157
		-15.0	-0.294	-0.106	-0.076
		-20.0	-0.331	-0.345	0.018
		-25.0	-0.515	-0.418	0.063
		-30.0	-0.496	-0.455	0.093
		-35.0	-0.588	-0.326	0.157
		-35.0	-0.625	-0.547	0.131
		-30.0	-0.460	-0.492	0.129
		-25.0	-0.441	-0.400	0.076
		-20.0	-0.349	-0.291	0.030
		-15.0	-0.257	-0.193	-0.051
		-10.0	-0.202	0.005	-0.167
		-5.0	-0.129	0.060	-0.311
0.2045	0.0	0.0	-0.110	0.372	-0.445
0.2045	10.0	0.0	-0.563	3.451	-0.144
		-5.0	-0.361	3.250	0.008
		-10.0	-0.380	3.013	0.152
		-15.0	-0.471	2.942	0.303
		-20.0	-0.766	2.723	0.427
		-25.0	-0.858	2.496	0.553
		-30.0	-0.876	2.362	0.619
0.2045	10.0	-35.0	-1.005	2.189	0.639

TABLE 7 (Cont)

Data from Rotating-Arm Tests for 10-Knot Condition

$$(F = \frac{U}{\sqrt{gL}} = 0.1295, \quad J = \frac{U}{nD} = 0.979)$$

(Values for Coefficients X', Y', and N' must be multiplied by 10^{-3})

r'	β deg	δ_R deg	X'	Y'	N'
0.2045	20.0	0.0	-0.529	7.886	-0.144
		-5.0	-0.474	7.595	0.035
		-10.0	-0.603	7.286	0.192
		-15.0	-0.584	6.819	0.369
		-19.9	-0.676	6.545	0.515
		-25.0	-0.805	6.345	0.662
		-30.0	-0.897	6.519	0.765
		-35.0	-1.025	6.530	0.841
		-35.0	-1.246	6.357	0.780
		-30.0	-1.117	6.603	0.735
		-25.0	-1.007	6.439	0.647
		-20.0	-0.897	6.633	0.493
		-15.0	-0.860	6.838	0.374
		-10.0	-0.786	7.159	0.205
		-5.0	-0.676	7.556	0.063
0.2045	20.0	0.0	-0.639	8.019	-0.124
0.6246	-5.0	0.0	0.240	0.279	-1.980
		-5.0	0.295	0.298	-1.773
		-10.0	0	-0.144	-1.662
		-15.0		0.171	-1.546
		-20.0	-0.018	-0.769	-1.384
		-25.0	0.074	-0.511	-1.288
		-30.0	•	-1.273	-1.202
		-35.1		-0.849	-1.243
		-30.0	0.220	-1.735	-1.273
0.6246	-5.0	-35.0	-0.165		-1.177
0.6246	0.0	0.0	-0.055	2.026	-1.743
		-5.0	-0.055		-1.586
		-10.0	-0.129	1.477	-1.520
		-15.0	-0.165	2.056	-1.313
		-20.0	-0.202	1.007	-1.217
		-25.0	-0.257	0.808	-1.015
		-30.0	-0.368	1.175	-0.889
		-35.0	-0.460	0.375	-0.914
		-5.0	-0.037	1.504	-1.611

TABLE 7 (Cont)

Data from Rotating-Arm Tests for 10-Knot Condition

$$(F = \frac{U}{\sqrt{gL}} = 0.1295, \quad J = \frac{U}{nD} = 0.979)$$

(Values for Coefficients X', Y', and N' must be multiplied by 10^{-3})

r'	β deg	δ_R deg	X'	Y'	N'
		-15.0	-0.055	1.543	-1.243
		-30.0	-0.313	1.258	-0.854
	0.0		0.074	1.995	-1.758
		-12.5	-0.055	1.382	-1.409
		-17.5	-0.110	1.325	-1.273
		-27.5	-0.313	0.527	-0.934
		-32.5	-0.349	0.692	-0.884
		-30.0	-0.349	0.767	-0.924
		-7.5	0.018	1.815	-1.490
		-2.5	0.037	2.156	-1.702
		-5.0	0.018	2.100	-1.556
0.6246	0.0	-10.0	0.018	1.913	-1.424
0.6246	5.0	0.0	-0.515	4.347	-1.727
		-5.1	-0.479	4.711	-1.546
		-9.9	-0.534	3.599	-1.429
		-15.0	-0.589	3.950	-1.217
		-20.0	-0.626	2.865	-1.101
		-24.9	-0.607	3.144	-0.909
		-30.0	-0.865	2.725	-0.808
		-35.0	-0.901	3.044	-0.743
		-5.0	-0.396	3.885	-1.500
		-15.0	-0.570	3.723	-1.157
		0.0	-0.442	4.354	-1.672
		-20.0	-0.534	2.584	-1.020
		-25.0	-0.644	2.937	-0.917
		-17.5	-0.552	3.328	-1.131
		-30.0	-0.736	2.468	-0.813
		-34.8	-0.809	2.476	-0.743
0.6246	5.0	-24.9	-0.607	3.162	-0.823
0.6246	10.0	0.0	-0.795	7.144	-1.828
		-5.0	-0.813	7.082	-1.647
		-10.0	-0.868	6.313	-1.470
		-15.0	-0.978	6.240	-1.344
		-20.0	-1.043	5.651	-1.145
		-25.0	-1.144	5.210	-1.005

TABLE 7 (Cont)

Data from Rotating-Arm Tests for 10-Knot Condition

$$\left(F = \frac{U}{\sqrt{gL}} = 0.1295, \quad J = \frac{U}{nD} = 0.979\right)$$

(Values for Coefficients X', Y', and N' must be multiplied by 10^{-3})

r'	β deg	δ_R deg	X'	Y'	N'
		-29.9	-1.291	5.126	-0.975
		-35.0	-1.346	5.148	-0.884
		-5.0	-0.813	6.656	-1.642
		-15.0	-0.905	5.973	-1.303
0.6246	10.0	-5.0	-0.702	6.807	-1.687
0.6246	15.0	0.0	-0.914	9.737	-2.106
		-5.0	-0.933	9.428	-1.894
		-10.0	-1.006	8.939	-1.667
		-15.1	-1.080	8.804	-1.515
		-20.0	-1.172	8.293	-1.318
		-25.0	-1.245	7.671	-1.162
		-30.0	-1.374	7.677	-1.030
		-35.0	-1.484	7.216	-0.945
0.6246	15.0	-25.0	-1.209	7.659	-1.126
0.6246	20.0	0.0	-1.210	12.783	-2.465
		-5.0	-1.173	12.303	-2.238
		-10.0	-1.320	12.147	-2.081
		-15.0	-1.265	11.590	-1.818
		-20.0	-1.430	11.446	-1.672
		-25.0	-1.467	11.117	-1.475
		-30.0	-1.614	10.726	-1.379
		-35.0	-1.669	10.492	-1.253
		-15.0	-1.338	11.549	-1.874
		-5.0	-1.246	12.908	-2.329
0.6246	20.0	-15.0	-1.338	11.708	-1.859

TABLE 8

Rotating-Arm Test Data for Model without Propeller for Tangential Speed of 20 Knots ($F = \frac{U}{\sqrt{gL}} = 0.259$)

(Values for Coefficients X', Y', and N' must be multiplied by 10^{-3})

r'	β degrees	δ_R degrees	X'	Y'	N'
0.2045	0.0	0.0	-0.641	-0.012	-0.521
		-5.0	-0.643	-0.083	-0.456
		-10.0	-0.669	-0.106	-0.400
		-15.0	-0.669	-0.200	-0.345
		-20.0	-0.780	-0.172	-0.234
		-25.0	-0.775	-0.125	-0.177
		-30.0	-0.844	-0.250	-0.132
		-35.0	-0.839	-0.242	-0.119
		-20.0	-0.835	-0.093	-0.225
		-35.0	-0.862	-0.224	-0.132
		-35.0	-0.918	-0.263	-0.118
		-30.0	-0.816	-0.206	-0.137
		-25.0	-0.761	-0.178	-0.184
		-15.0	-0.632	-0.222	-0.328
		-10.0	-0.632	-0.143	-0.395
		-5.0	-0.618	-0.032	-0.443
0.2045	0.0	0.0	-0.599	0.060	-0.502

TABLE 9

Rotating-Arm Test Data for Propeller Advance Coefficient Variation for Tangential Speed of 20 Knots ($F = \frac{U}{\sqrt{gL}} = 0.259$) and Radius of 106.79 Ft ($r' = 0.2045$)

(Values for Coefficients X', Y', and N' must be multiplied by 10^{-3})

$J = \frac{U}{nD}$	β degrees	δ_R degrees	X'	Y'	N'
0.652	0.0	0.0	1.328	0.263	-0.590
0.783			0.512	0.187	-0.583
0.979			-0.129	0.110	-0.573
1.307			-0.540	0.050	-0.547
1.957			-0.913	-0.017	-0.498
3.931	0.0	0.0	-1.337	-0.067	-0.455
0.652	0.0	-35.0	0.441	-1.072	0.395
0.979	0.0	-35.0	-0.540	-0.524	0.084

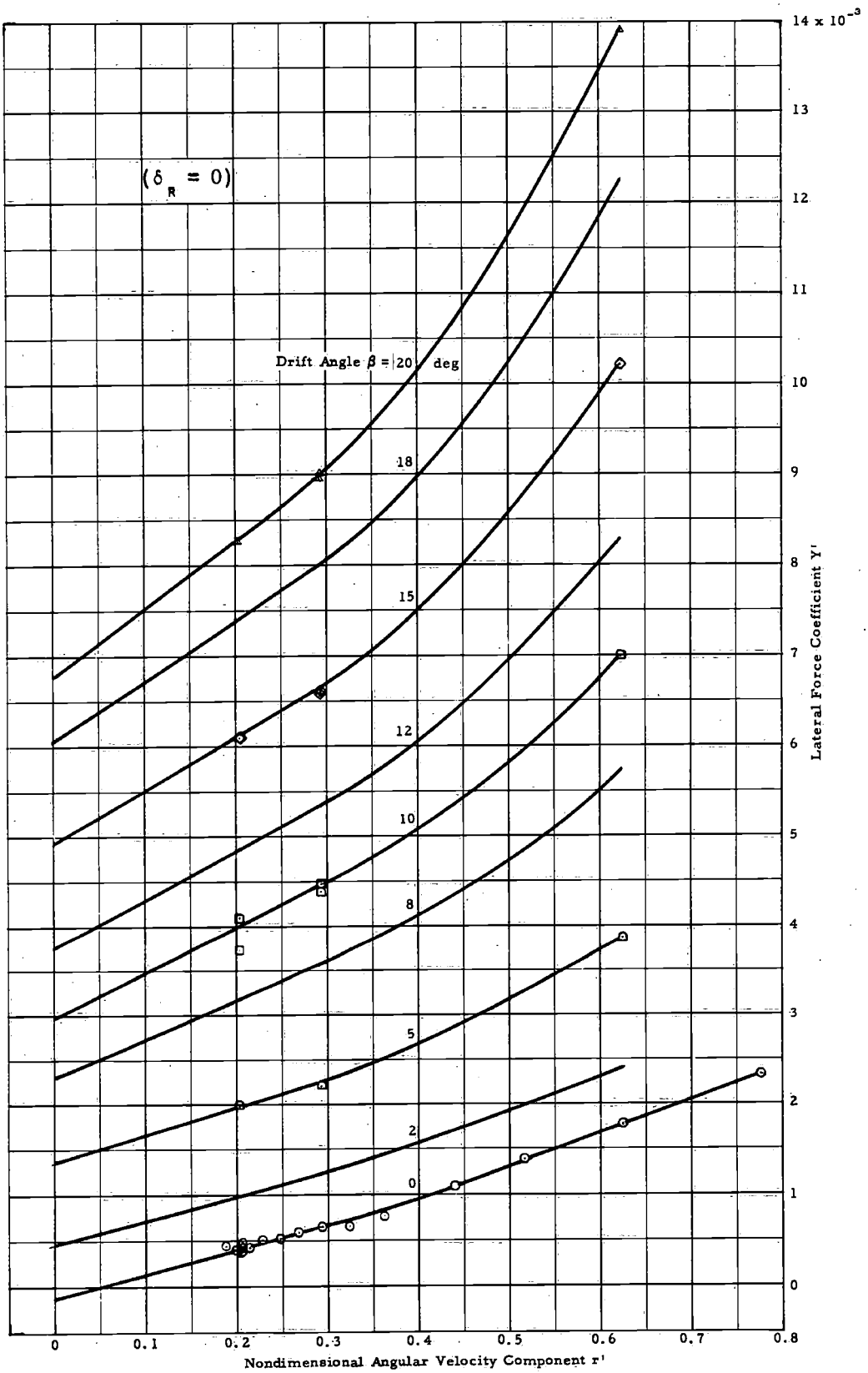

Figure 15 - Lateral Force as a Function of Angular Velocity for Various Drift Angles (20-Knot Condition)

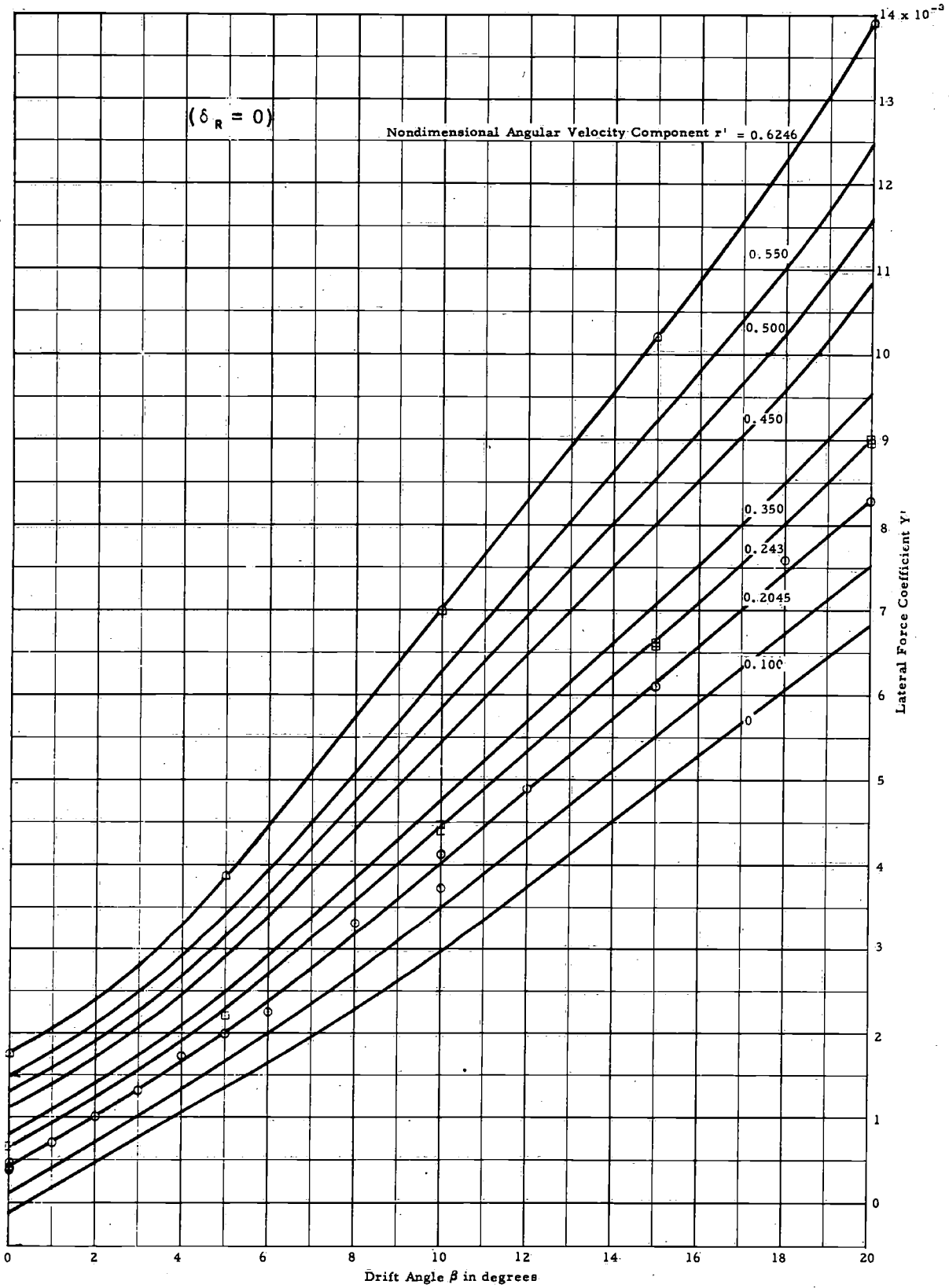

Figure 16 - Lateral Force as a Function of Drift Angle for Various Angular Velocities (20-Knot Condition)

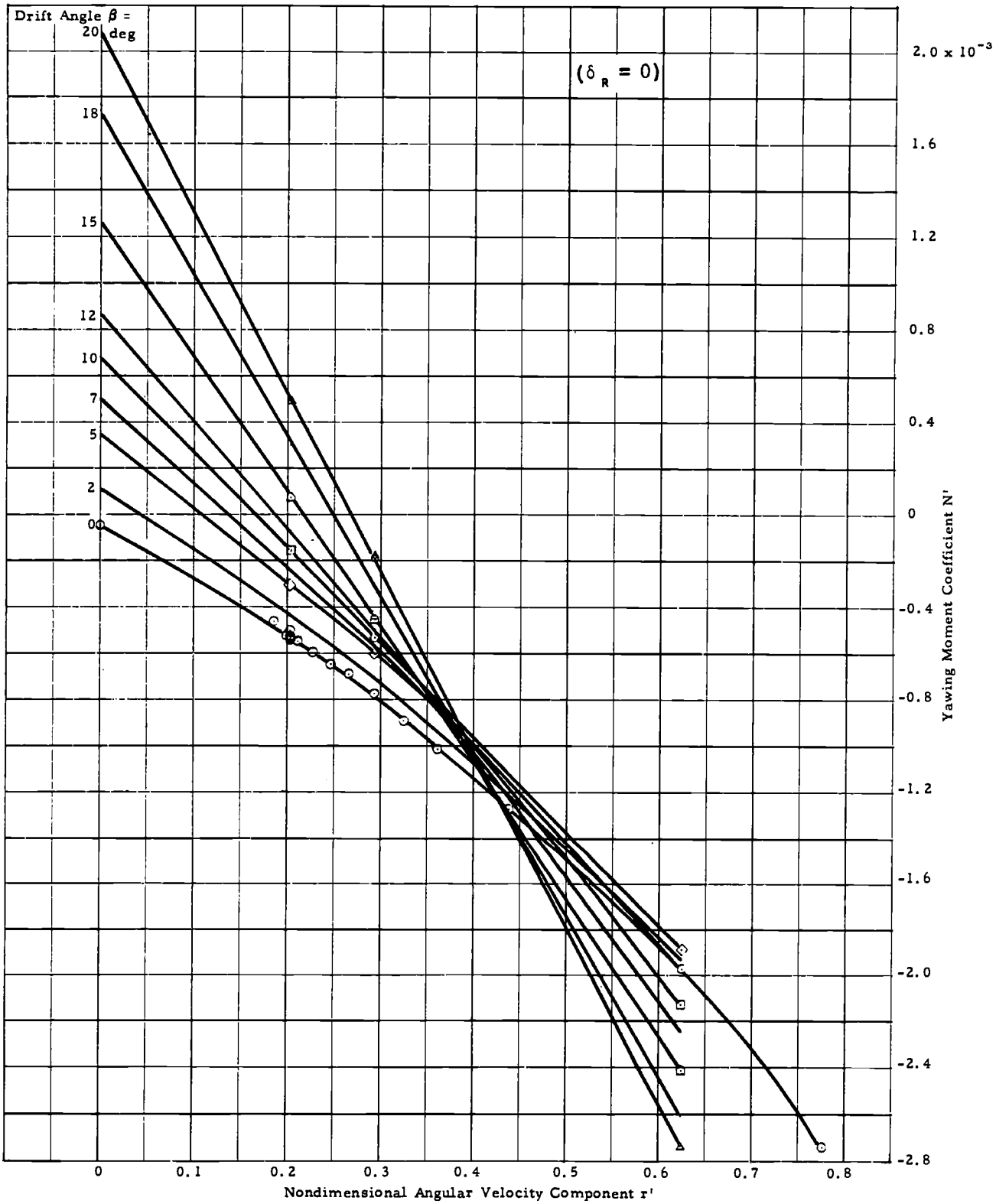

Figure 17 - Yawing Moment as a Function of Angular Velocities for Various Drift Angles (20-Knot Condition)

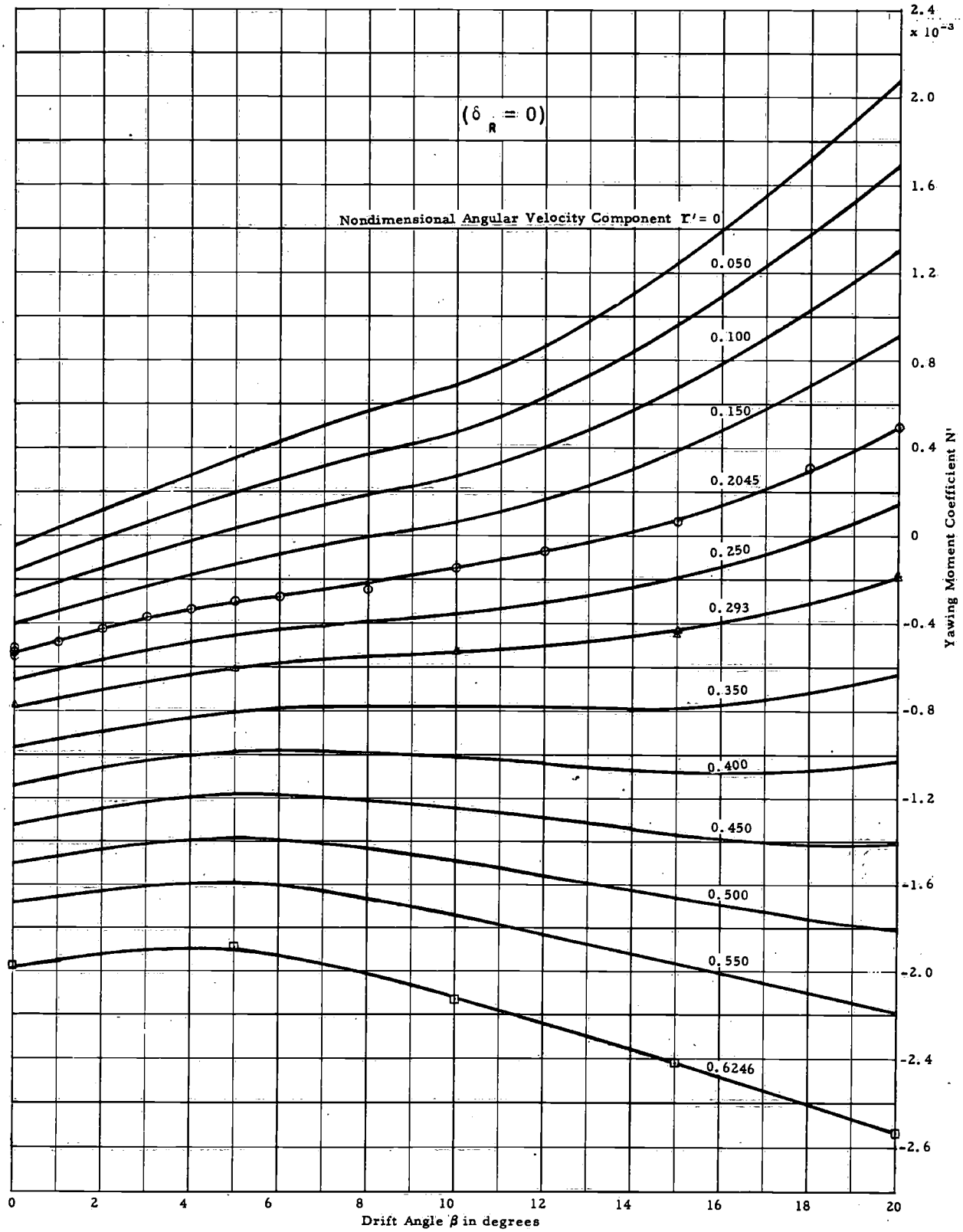

Figure 18 - Yawing Moment as a Function of Drift Angle for Various Angular Velocities (20-Knot Condition)

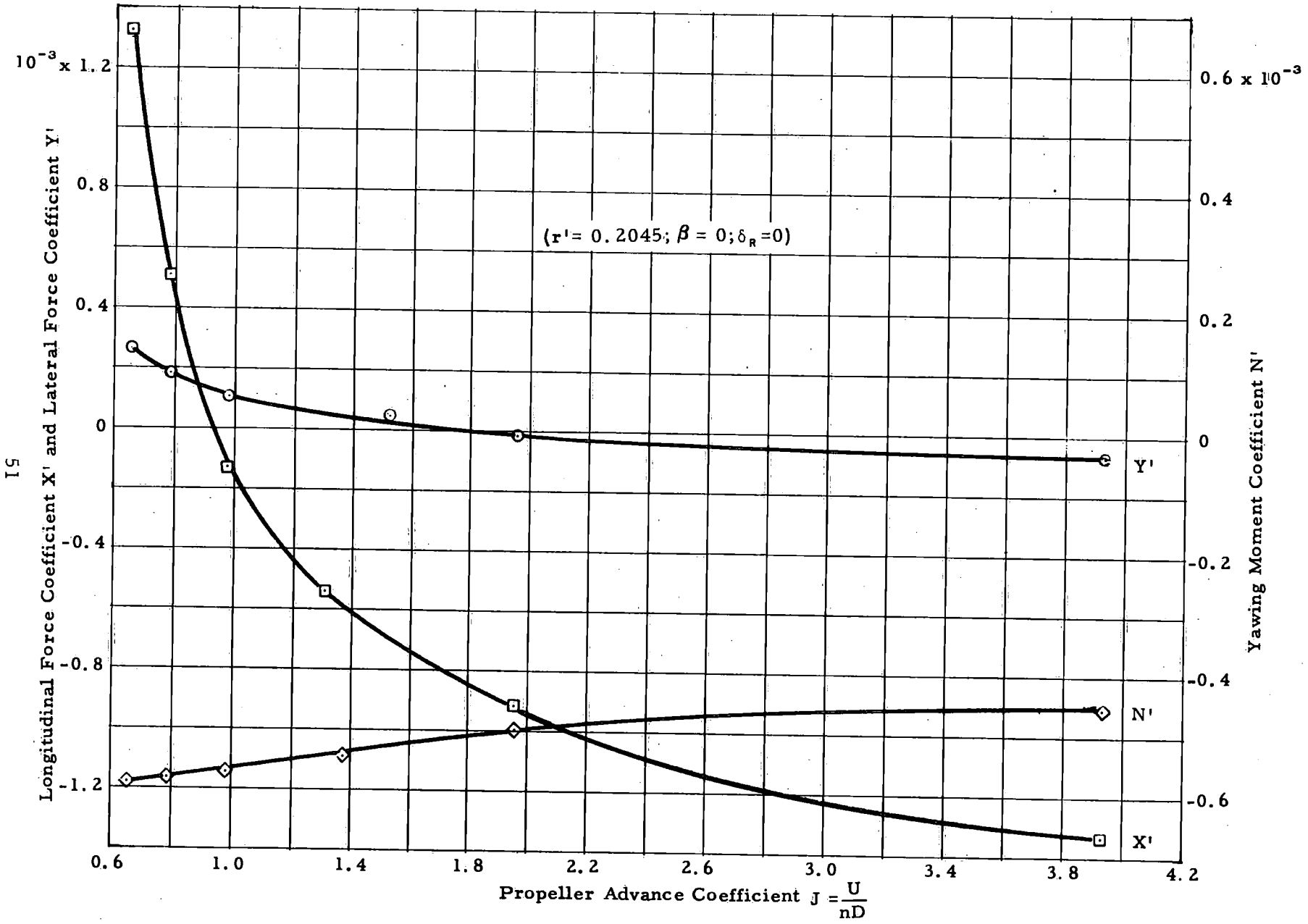

Figure 19 - Variation of Hydrodynamic Coefficients X', Y', and N' with Propeller Advance Coefficient J (20-Knot Condition)

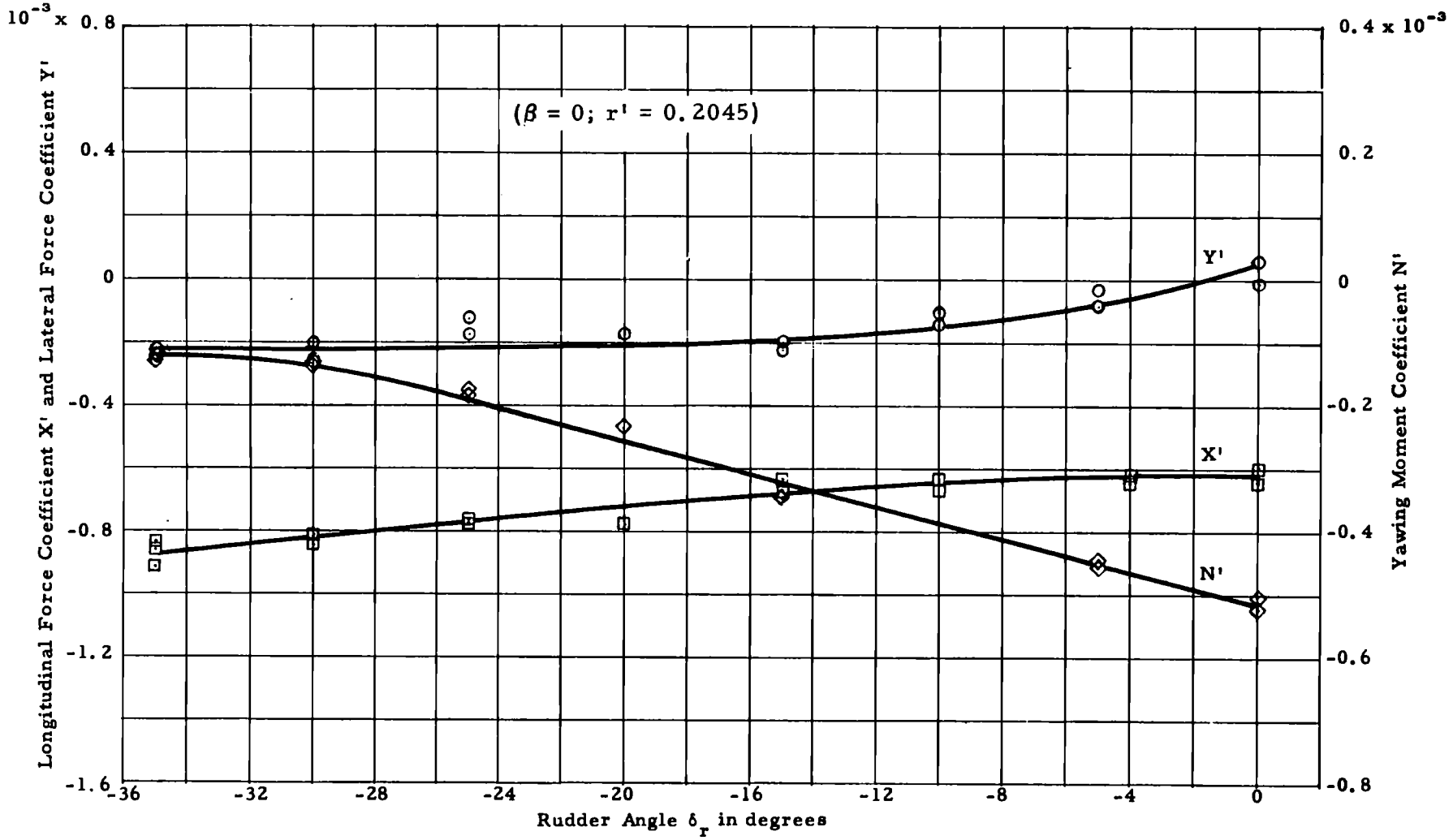

Figure 20 - Variation of Hydrodynamic Coefficients X', Y', and N' with Rudder Angle δ_R (without Propeller at 20-Knot Condition)

APPENDIX B

HYDRODYNAMIC DATA OBTAINED FROM STRAIGHTLINE TESTS

(Tables 10 through 11 and Figures 21 through 32)

TABLE 10

Data from Straightline Tests for 20-Knot Condition

$$\left(F = \frac{U}{\sqrt{gL}} = 0.259, \quad J = \frac{U}{nD} = 0.979\right)$$

(Values for Coefficients X', Y', and N' must be multiplied by 10^{-3})

β deg	δ_R deg	X'	Y'	N'
0.0	0.0	-0.046	-0.155	-0.047
	-5.0	-0.018	-0.298	0.110
	-10.1	-0.065	-0.466	0.230
	-15.1	-0.097	-0.683	0.339
	-19.9	-0.161	-0.883	0.470
	-25.0	-0.309	-0.860	0.462
	-30.0	-0.392	-0.895	0.490
	-35.0	-0.484	-0.970	0.522
	0.0		-0.242	-0.077
	-4.9		-0.377	0.079
	-10.1		-0.645	0.205
	-14.9		-0.816	0.339
	-19.9		-0.899	0.493
	-25.1	-0.272	-0.930	0.481
	-30.0	-0.346	-0.983	0.521
	-34.8	-0.424	-1.034	0.569
	0.1	0.046	-0.201	-0.077
	5.0	0.042	0.007	-0.223
	10.0	0.023	0.290	-0.325
	15.1	-0.032	0.532	-0.458
0.0	20.0	-0.037	0.822	-0.575
5.0	0.0	-0.032	1.430	0.363
	-5.0	-0.018	1.148	0.496
	-9.9	-0.074	0.871	0.603
	-15.0	-0.101	0.606	0.729
	-19.9	-0.161	0.353	0.824
	-25.0	-0.230	0.172	0.883
	-29.9	-0.387	0.092	0.920
5.0	-35.1	-0.489	0.217	0.964

TABLE 10 (Cont)

Data from Straightline Tests for 20-Knot Condition

$$\left(F = \frac{U}{\sqrt{gL}} = 0.259, \quad J = \frac{U}{nD} = 0.979\right)$$

(Values for Coefficients X', Y', and N' must be multiplied by 10^{-3})

β deg	δ_R deg	X'	Y'	N'
10.0	0.0	-0.152	2.866	0.662
	-5.0	-0.148	2.772	0.855
	-10.0	-0.171	2.402	0.959
	-15.0	-0.235	2.727	1.102
	-20.1	-0.332	2.052	1.279
	-25.0	-0.369	1.912	1.389
	-30.0	-0.479	1.795	1.466
10.0	-34.9	-0.622	1.656	1.422
15.0	0.0	-0.180	5.470	1.292
	-5.0	-0.244	5.409	1.488
	-10.0	-0.263	4.981	1.586
	-15.0	-0.309	4.713	1.741
	-20.0	-0.415	4.365	1.849
	-25.0	-0.498	4.237	2.007
	-29.9	-0.622	4.357	2.105
15.0	-35.0	-0.673	3.831	2.074
-6.4	0.0	-0.078	-1.913	-0.548
	5.1	-0.097	-2.159	-0.403
	-10.1	-0.143	-2.387	-0.275
	-15.1	-0.198	-2.555	-0.095
	-20.0	-0.364	-2.734	-0.001
	-25.1	-0.502	-2.894	0.046
	-30.0	-0.599	-3.066	0.080
-6.4	-35.0	-0.714	-3.092	0.114
-10.0	0.0	-0.143	-3.105	-0.899
	-4.9	-0.171	-3.420	-0.725
	-10.0	-0.184	-3.675	-0.554
	-14.9	-0.244	-3.815	-0.399
	-20.0	-0.415	-3.909	-0.250
	-25.0	-0.576	-3.993	-0.177
	-30.1	-0.742	-4.270	-0.108
-10.0	-35.1	-0.848	-4.374	-0.

TABLE 11

Data from Straightline Tests for 10-Knot Condition

$$(F = \frac{U}{\sqrt{gL}} = 0.1295,\ J = \frac{U}{nD} = 0.979)$$

(Values for Coefficients X', Y', and N' must be multiplied by 10^{-3})

β deg	δ_R deg	X'	Y'	N'
0.0	0.0	0.0	-0.074	-0.061
	-4.9	-0.037	-0.276	-0.098
	-10.0	-0.055	-0.546	0.207
	-14.9	-0.110	-0.785	0.311
	-19.9	-0.239	-0.914	0.389
	-25.0	-0.312	-0.963	0.457
	-30.1	-0.368	-1.152	0.497
	-35.0	-0.515	-1.123	0.510
	0.0	-0.055	0.086	-0.008
	5.0	-0.037	0.449	-0.098
	10.0	-0.055	0.590	-0.220
	15.0	-0.183	0.817	-0.366
0.0	20.0	-0.220	0.895	-0.513
5.0	0.0	-0.018	1.236	0.275
	-5.0	-0.147	0.942	0.427
	-10.1	-0.129	0.737	0.553
	-14.9	-0.165	0.162	0.636
	-19.9	-0.257	0.039	0.710
	-25.1	-0.312	-0.158	0.763
	-30.0	-0.423	-0.176	0.811
5.0	-34.9	-0.515	-0.127	0.843
10.0	0.0	-0.239	2.367	0.465
	-5.1	-0.239	2.115	0.601
	-10.1	-0.331	1.844	0.745
	-14.9	-0.294	1.721	0.874
	-19.8	-0.331	1.477	0.977
	-25.1	-0.460	0.968	1.023
	-29.9	-0.570	0.876	1.106
10.0	-35.1	-0.680	1.028	1.151

TABLE 11(Con't)

Data from Straightline Tests for 10-Knot Condition

$$(F = \frac{U}{\sqrt{gL}} = 0.1295,\ J = \frac{U}{nD} = 0.979)$$

(Values for Coefficients X', Y', and N' must be multiplied by 10^{-3})

β deg	δ_R deg	X'	Y'	N'
15.0	0.0	-0.331	4.571	0.682
	-5.0	-0.276	4.571	0.883
	-10.1	-0.331	4.112	0.997
	-15.1	-0.349	3.694	1.162
	-19.9	-0.349	3.411	1.288
	-25.1	-0.478	3.043	1.364
	-30.0	-0.588	3.135	1.477
15.0	-35.0	-0.680	3.411	1.515
20.0	0.0	-0.294	6.880	0.884
	-5.0	-0.294	6.880	1.098
	-10.0	-0.331	6.704	1.174
	-15.0	-0.404	7.029	1.427
	-20.0	-0.460	6.386	1.540
	-25.0	-0.515	5.769	1.629
	-30.0	-0.643	5.119	1.704
	-35.0	-0.680	5.119	1.730
	-15.0	-0.386	5.720	1.338
	0.0	-0.221	7.539	0.947
	-5.0	-0.239	6.930	1.124
	-10.0	-0.331	6.604	1.300
	-15.0	-0.349	6.746	1.452
	-20.0	-0.460	6.378	1.603
	-25.0	-0.570	5.777	1.667
	-30.0	-0.570	5.677	1.742
20.0	-35.0	-0.735	6.053	1.831
-6.4	0.0	-0.184	-1.517	-0.444
	-5.0	-0.147	-1.892	-0.316
	-9.9	-0.239	-1.984	-0.162
	-14.9	-0.386	-2.241	0.000
	-19.9	-0.460	-2.671	0.081
	-24.9	-0.515	-2.622	0.184
	-30.0	-0.625	-2.671	0.237
-6.4	-34.9	-0.754	-2.898	0.258

TABLE 11(Cont')

Data from Straightline Tests for 10-Knot Condition

$$(F = \frac{U}{\sqrt{gL}} = 0.1295,\ J = \frac{U}{nD} = 0.979)$$

(Values for Coefficients X', Y', and N' must be multiplied by 10^{-3})

β deg	δ_R deg	X'	Y'	N'
-10.0	0.0	-0.202	-2.285	-0.619
	-4.9	-0.276	-2.753	-0.492
	-10.0	-0.294	-2.979	-0.341
	-15.0	-0.368	-3.120	-0.189
	-19.9	-0.496	-3.304	-0.004
	-25.0	-0.607	-3.580	0.025
	-30.0	-0.735	-3.764	0.101
-10.0	-34.9	-0.882	-3.721	0.152

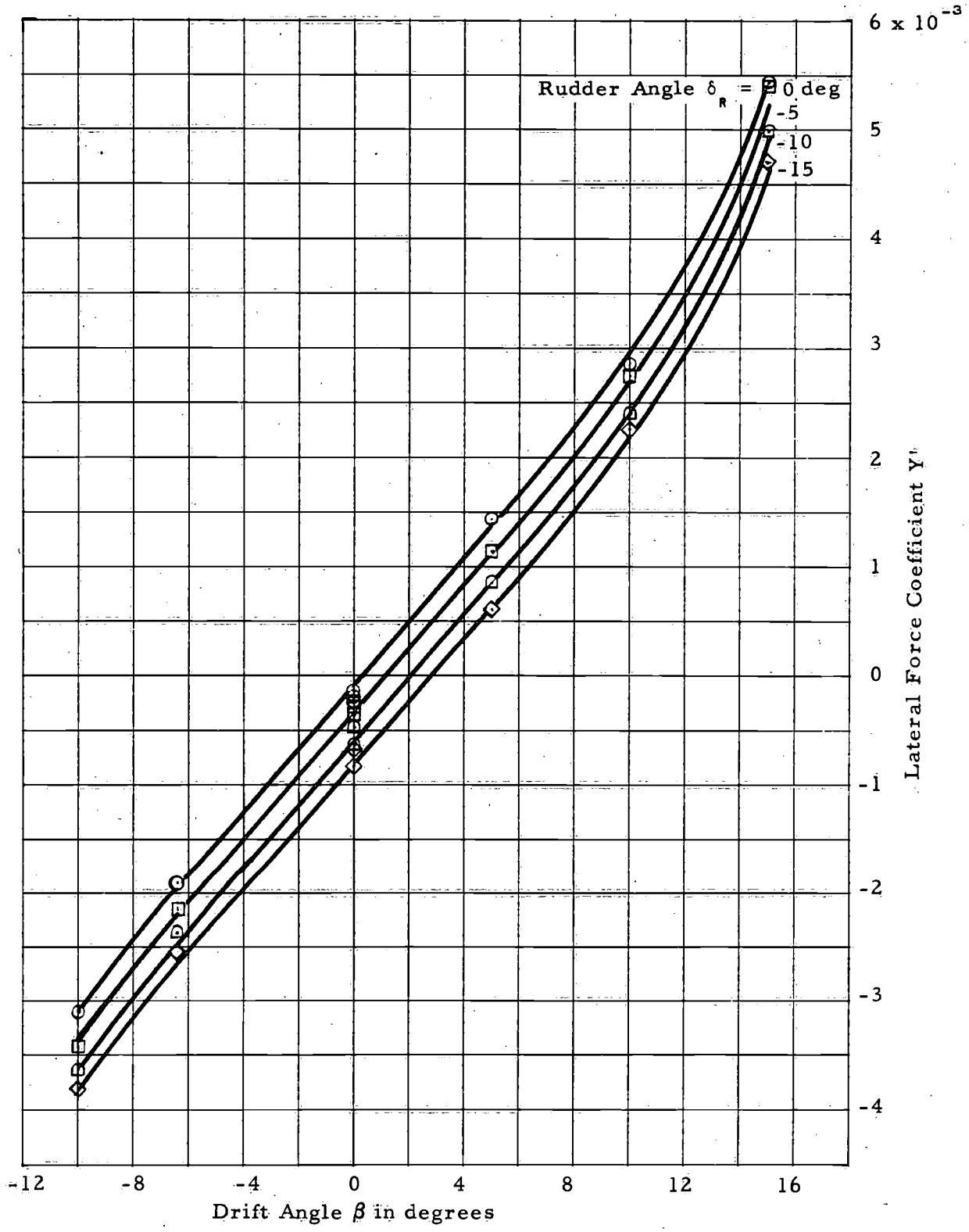

Figure 21 - Lateral Force as a Function of Drift Angle for Various Rudder Angles (20-Knot Condition)

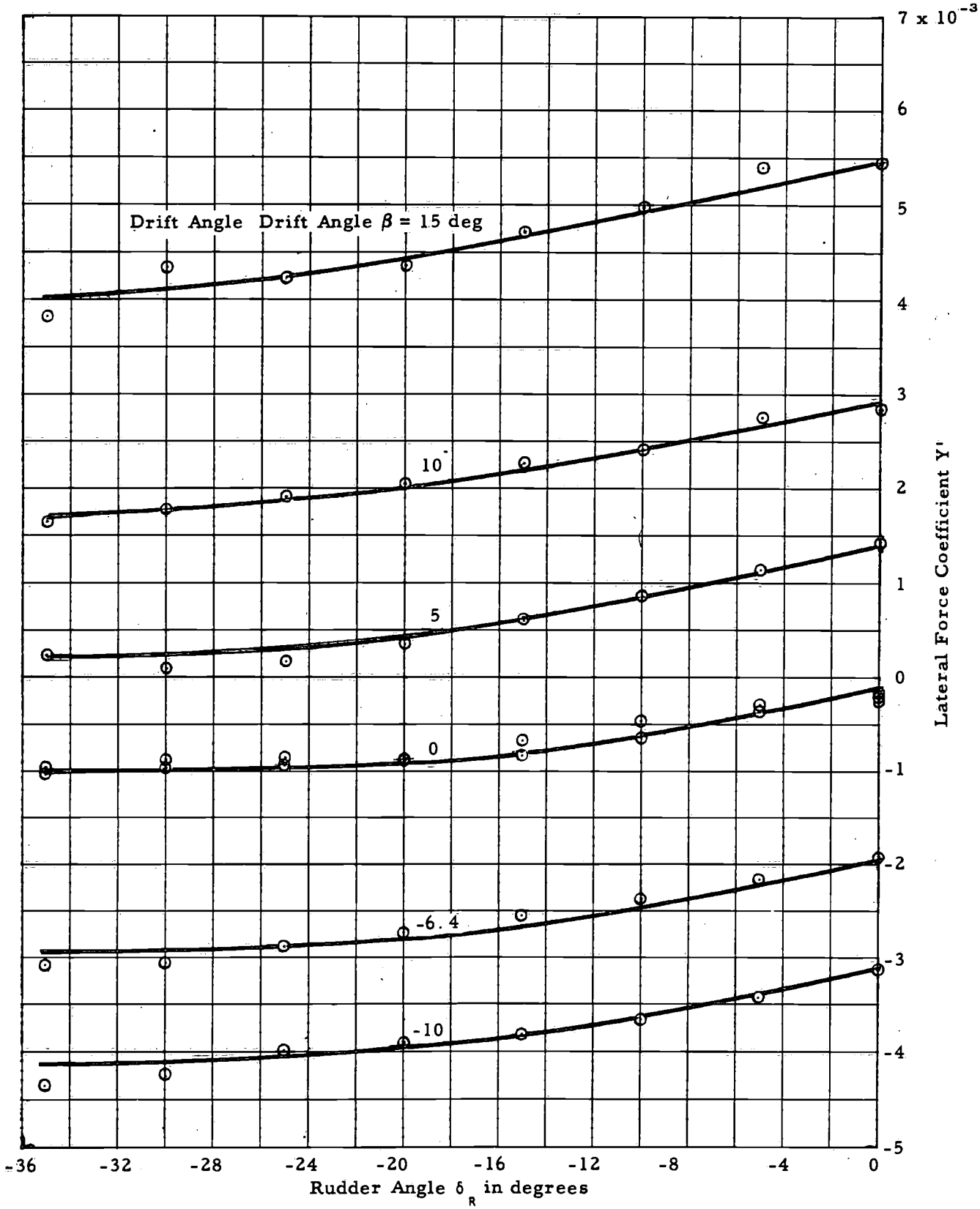

Figure 22 - Lateral Force as a Function of Rudder Angle for Various Drift Angles (20-Knot Condition)

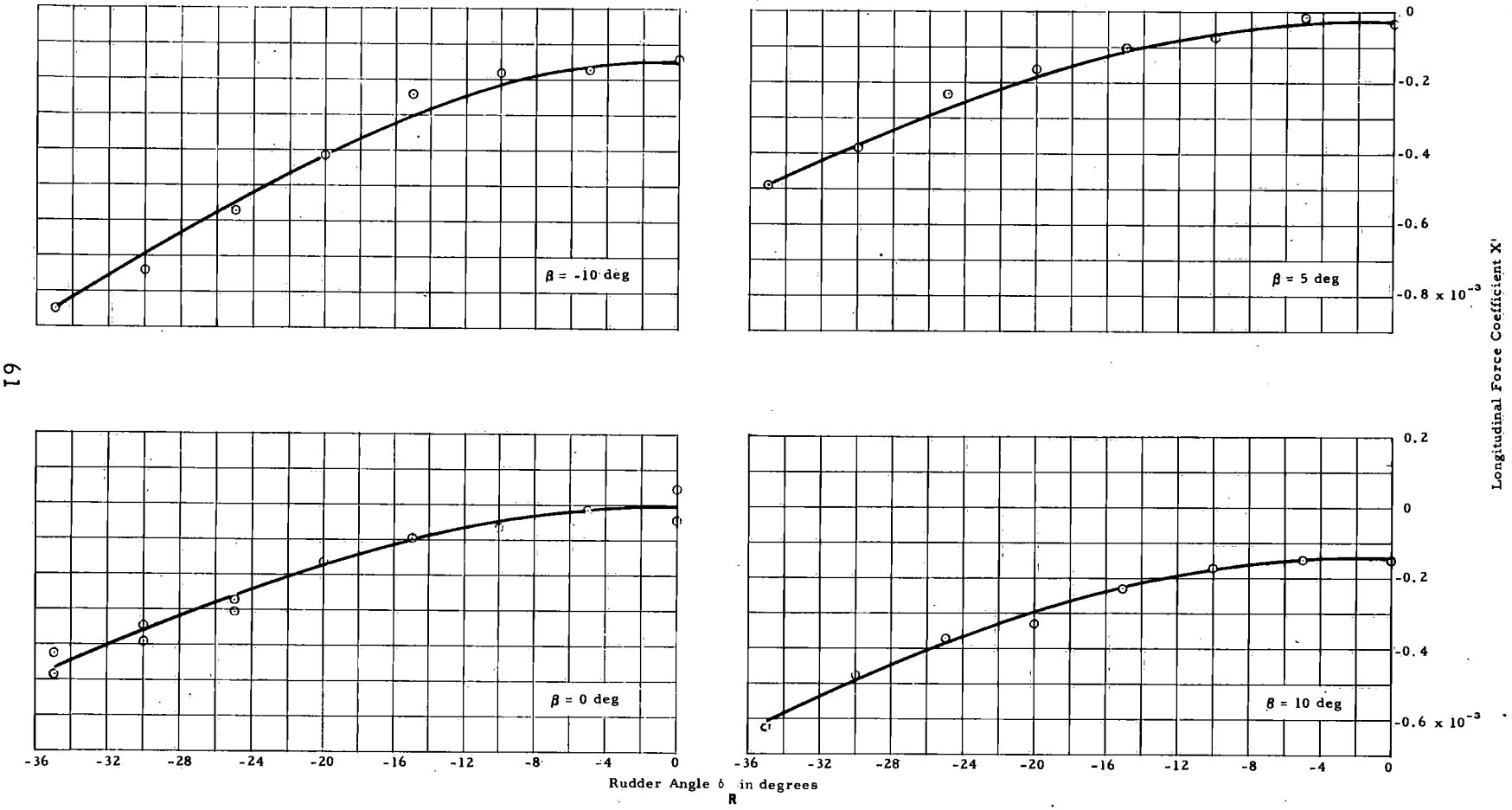

Figure 23 - Longitudinal Force as a Function of Rudder Angle for Various Drift Angles (20-Knot Condition)

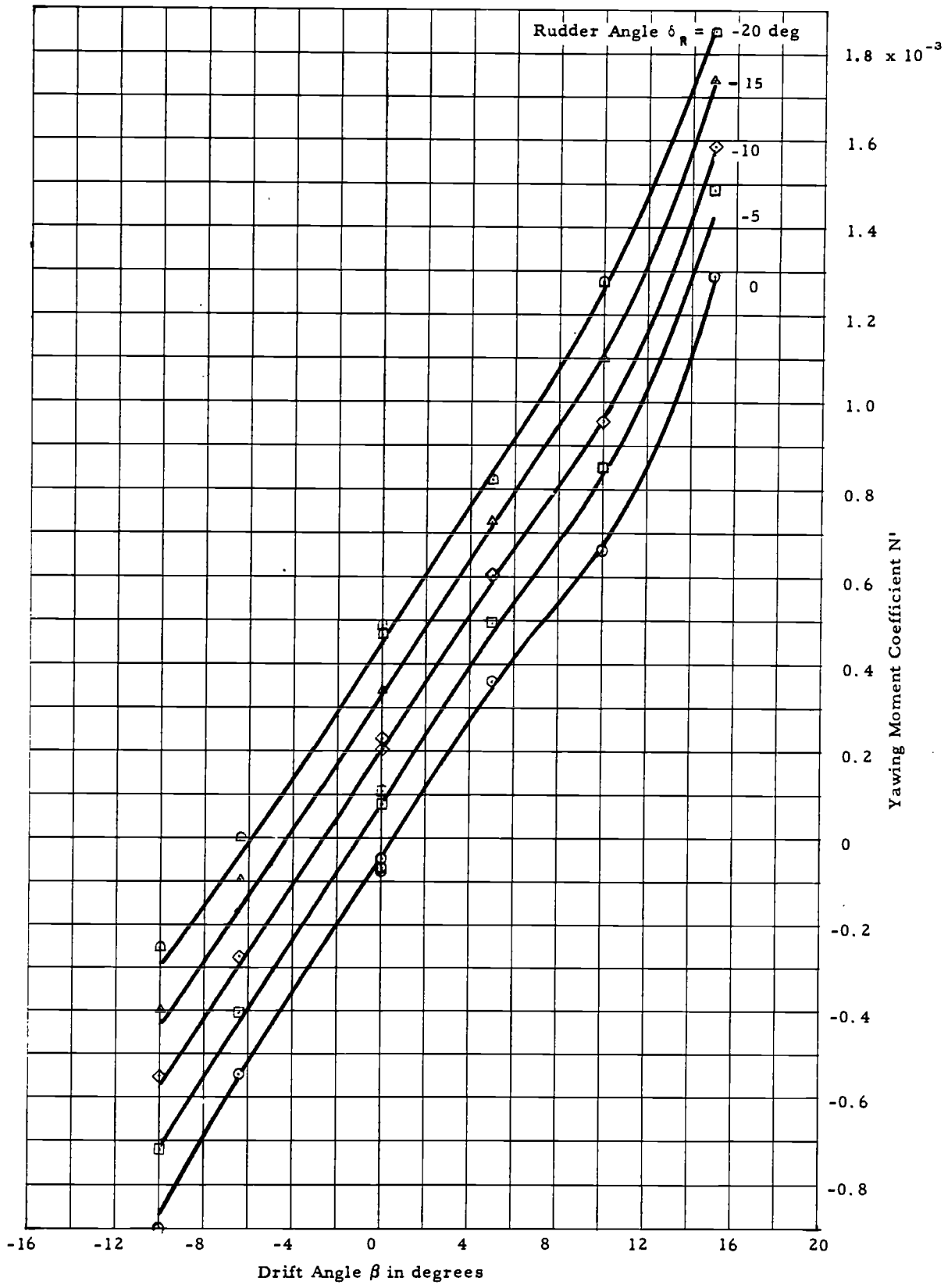

Figure 24 - Yawing Moment as a Function of Drift Angle for Various Rudder Angles (20-Knot Condition)

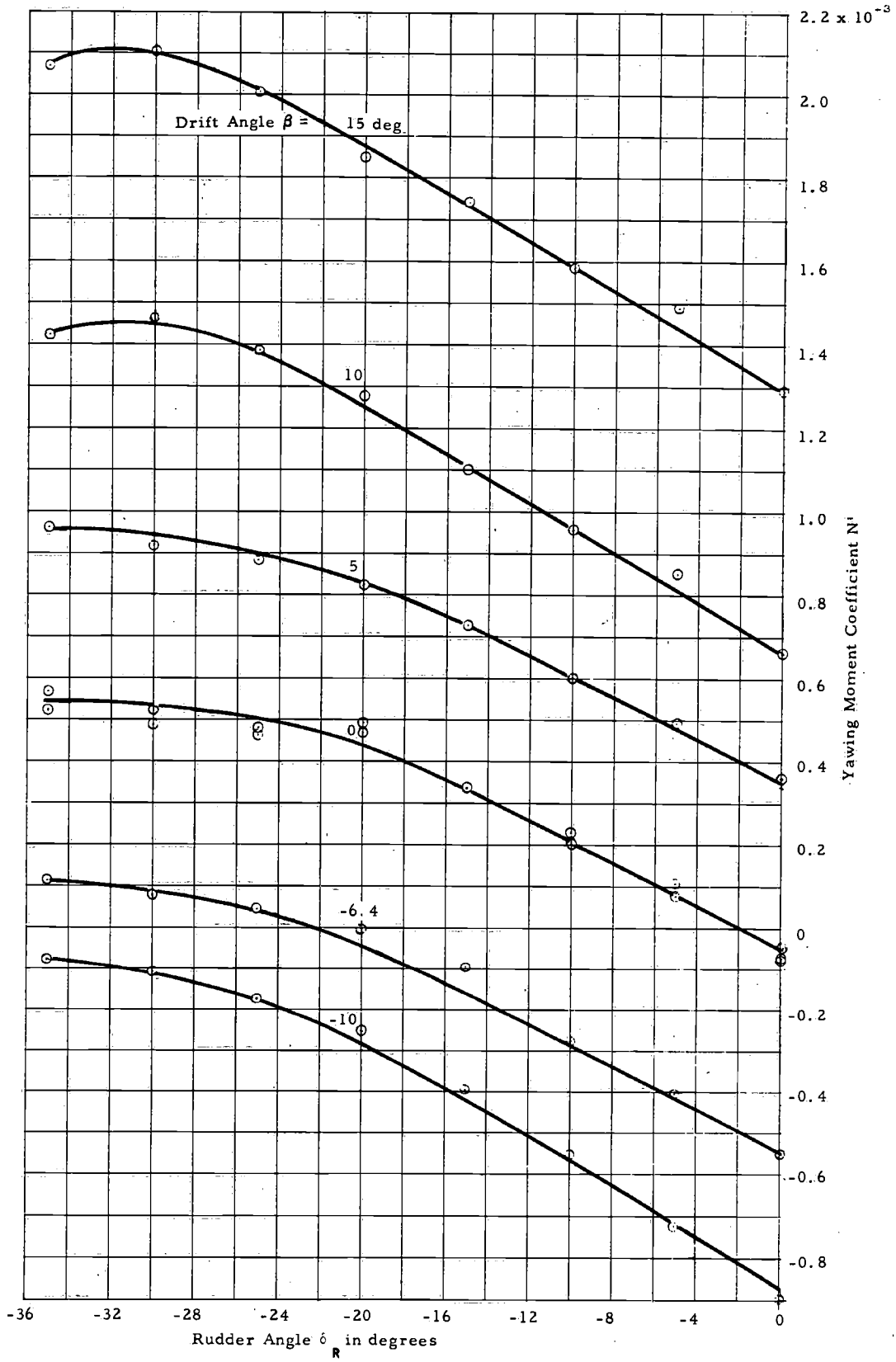

Figure 25 - Yawing Moment as a Function of Rudder Angle for Various Drift Angles (20-Knot Condition)

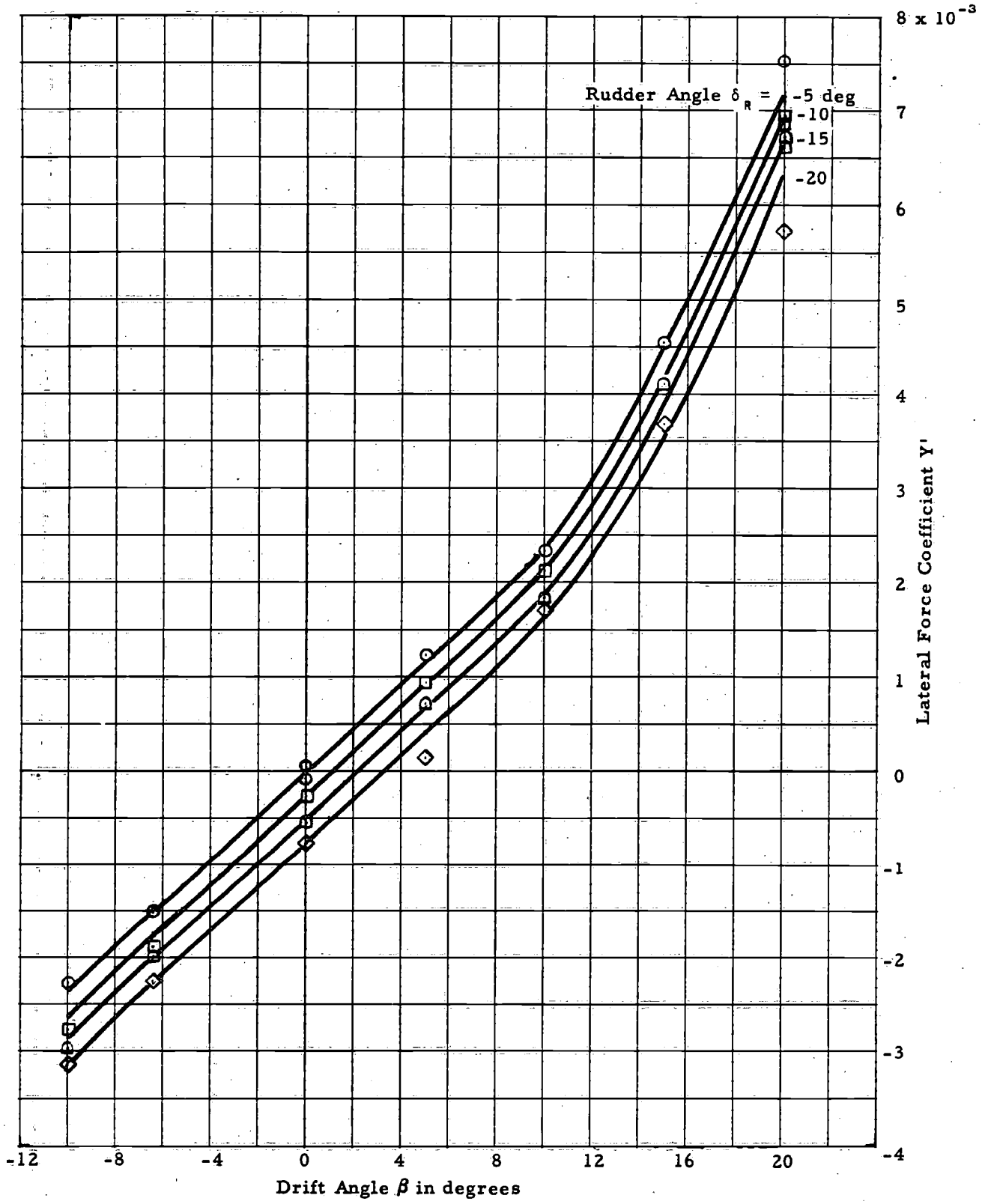

Figure 26 - Lateral Force as a Function of Drift Angle for Various Rudder Angles (10-Knot Condition)

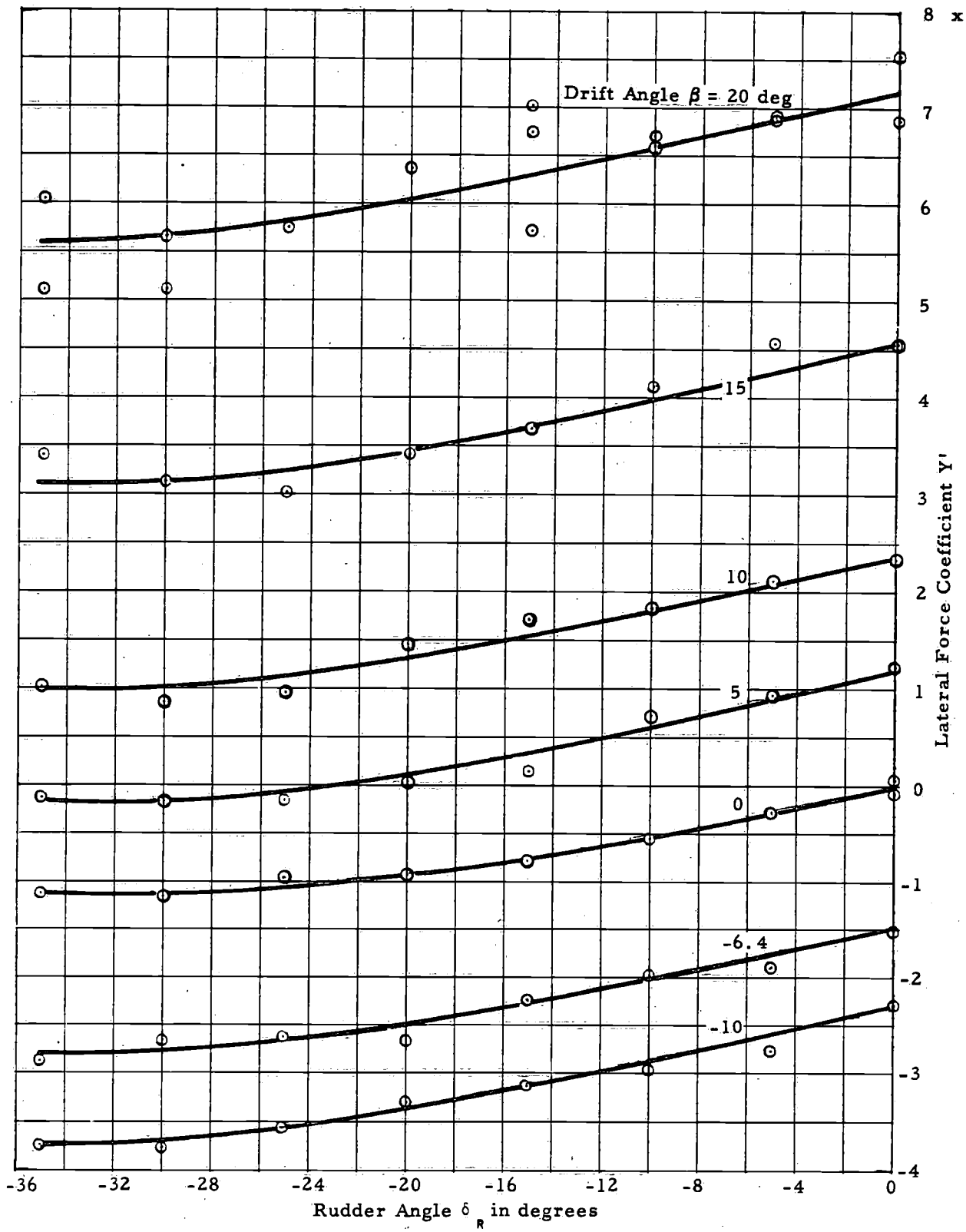

Figure 27 - Lateral Force as a Function of Rudder Angle for Various Drift Angles (10-Knot Condition)

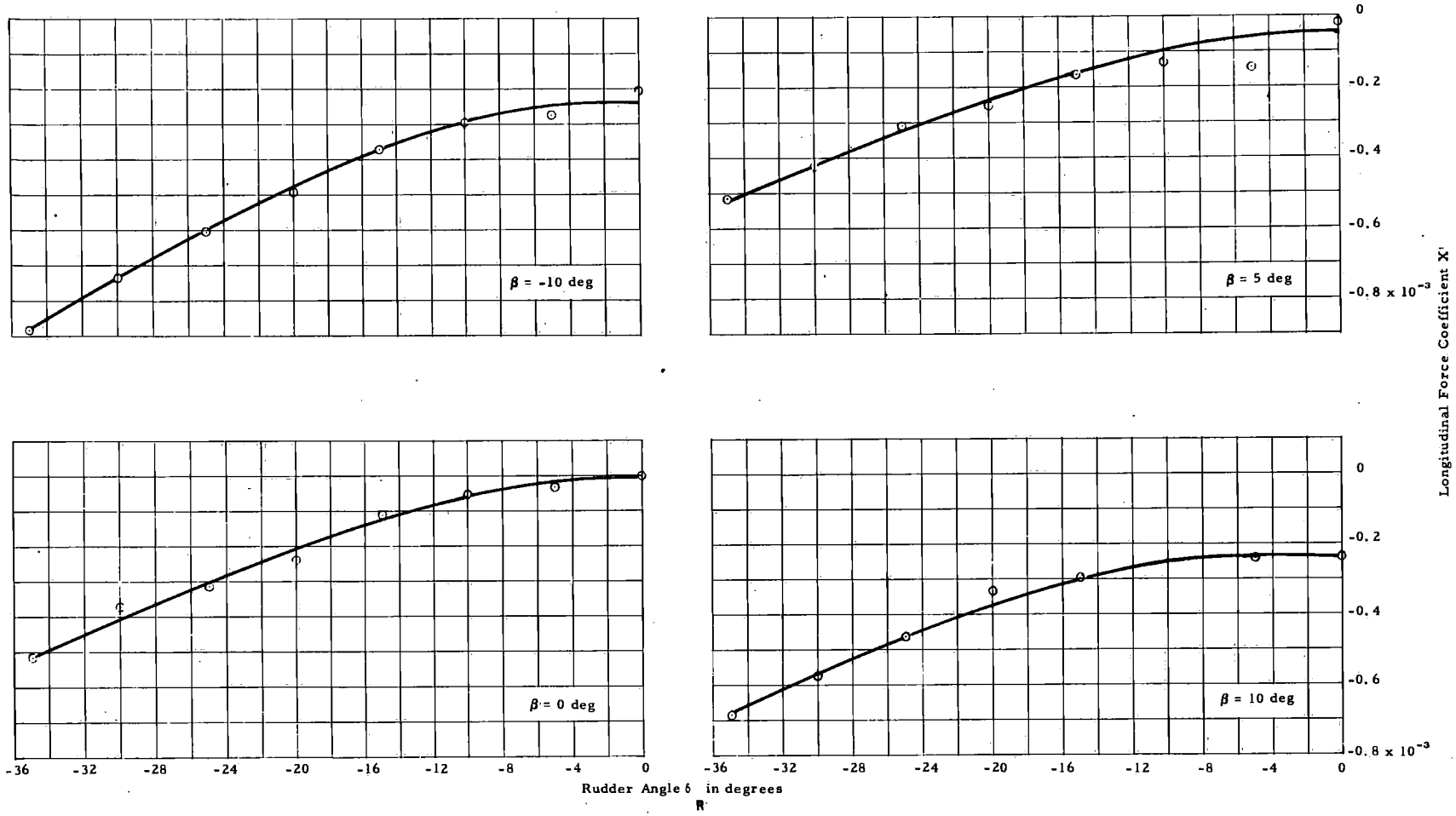

Figure 28 - Longitudinal Force as a Function of Rudder Angle for Various Drift Angles (10-Knot Condition)

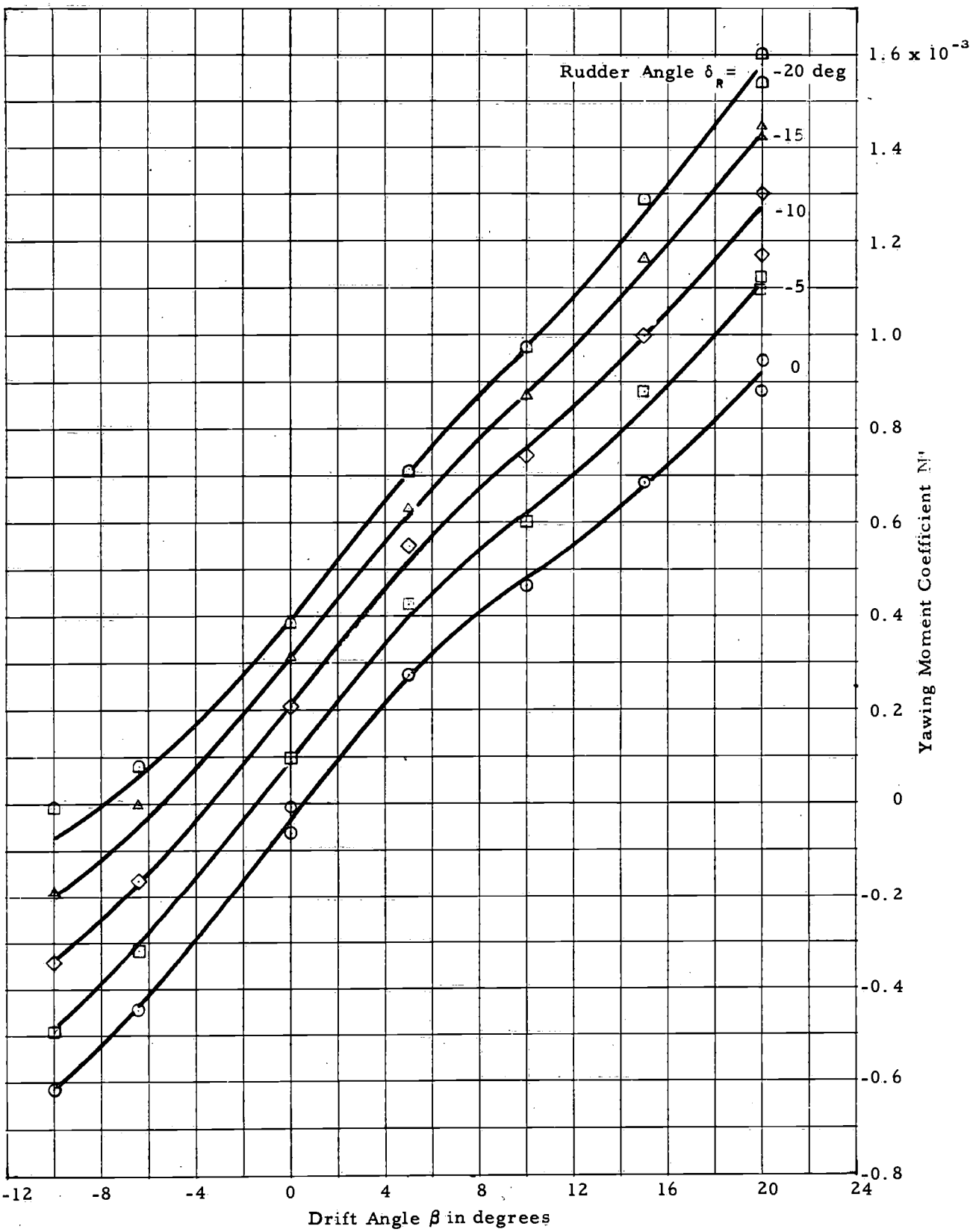

Figure 29 - Yawing Moment as a Function of Drift Angle for Various Rudder Angles (10-Knot Condition)

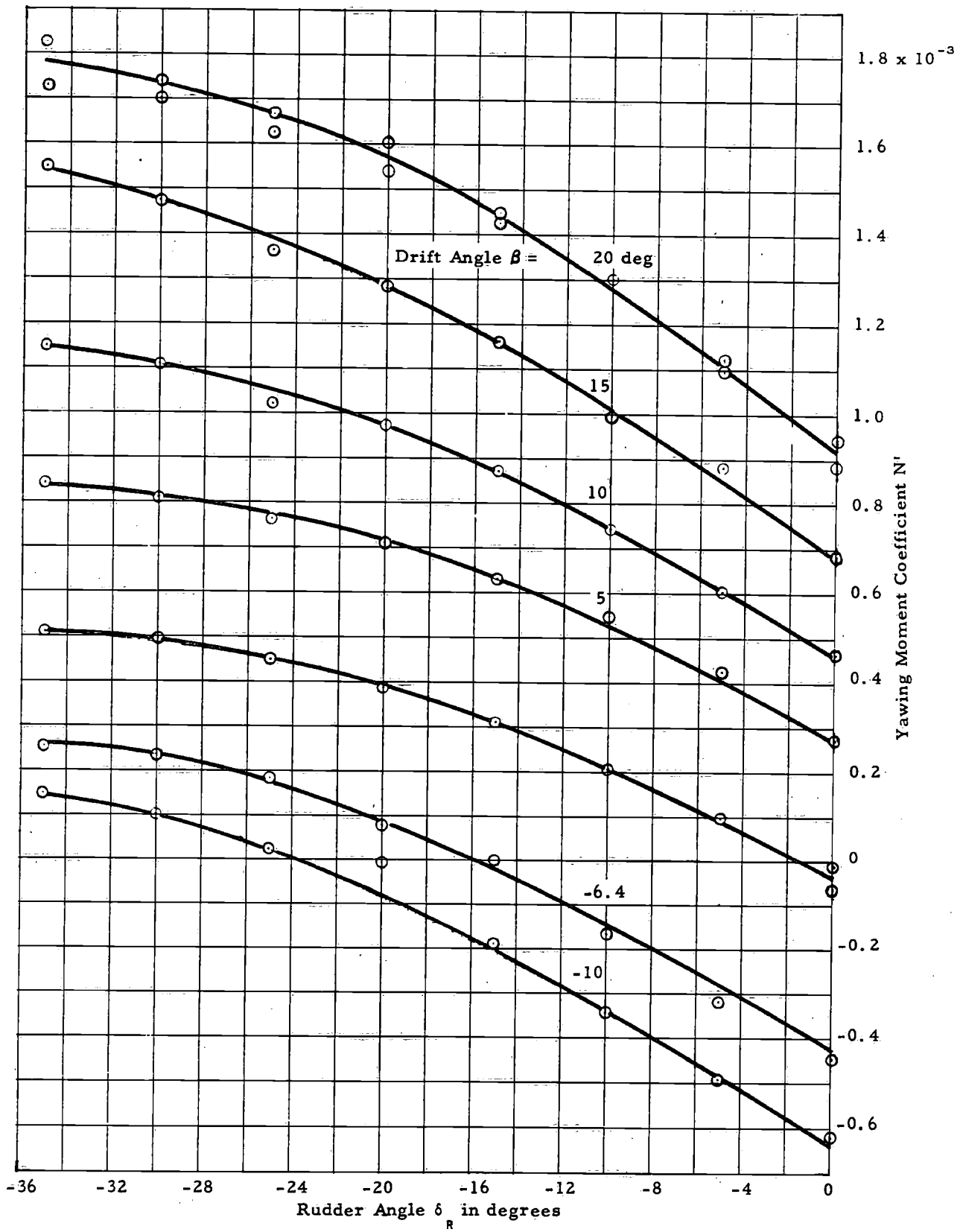

Figure 30 - Yawing Moment as a Function of Rudder Angle for Various Drift Angles (10-Knot Condition)

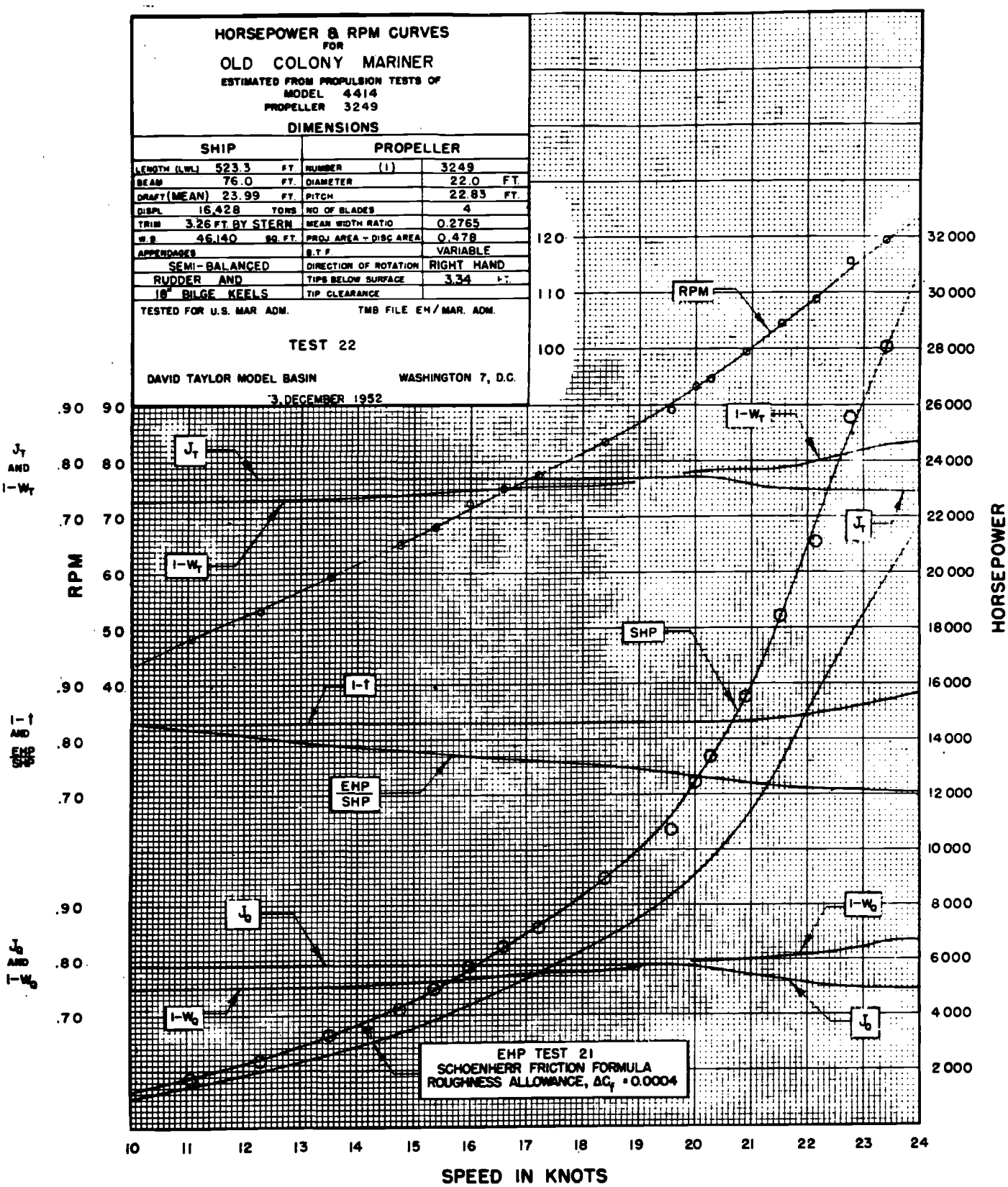

Figure 31 - Effective Horsepower, Shaft Horsepower and RPM for MARINER

CHARACTERISTIC CURVES
OF

PROPELLER	3249
TESTED FOR	U.S.M.A.
DESIGNED BY	U.S.M.A.
MARAD PLAN No.	1-25-S-44-0-1
DESIGN AGENT No.	C4SIA-38-9 ALT III
NUMBER OF BLADES	4
EXP. AREA RATIO	0.563
M W R	0.2765
B T F	0.0495
p÷d	1.038
DIAMETER	10.920 INS.
PITCH	11.334 INS.
ROTATION	R.H.
TEST RPM	696 RPM
TEST V_a	2.8 TO 7.1 KTS.

REYNOLD'S NO. $R_n = \frac{\sqrt{V_a^2 + (0.7\pi nd)^2}\, c}{\nu}$

THRUST COEFFICIENT, $K_1 = \frac{T}{\rho n^2 d^4}$

TORQUE COEFFICIENT, $K_q = \frac{Q}{\rho n^2 d^5}$

SPEED COEFFICIENT, $J = \frac{V_a}{nd}$

EFFICIENCY, $e = \frac{TV_a}{2\pi nQ} = \frac{K_1}{K_q} \cdot \frac{J}{2\pi}$

T = THRUST
Q = TORQUE
n = REVOLUTIONS PER UNIT TIME
V_a = SPEED OF ADVANCE
ν = KINEMATIC VISCOSITY
d = DIAMETER
p = PITCH
ρ = DENSITY OF WATER

14 APRIL 1952
DAVID W. TAYLOR MODEL BASIN
WASHINGTON, D.C

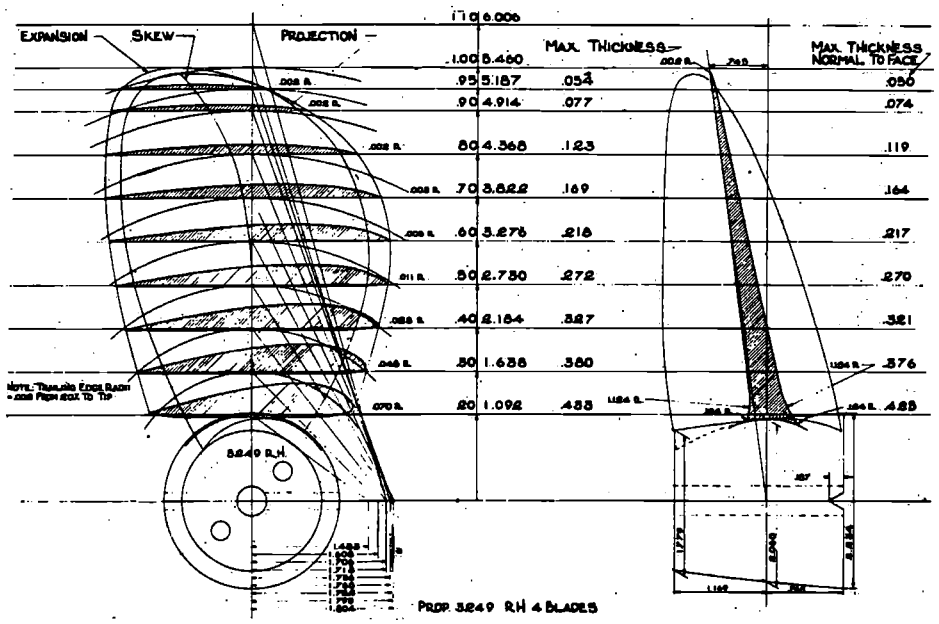

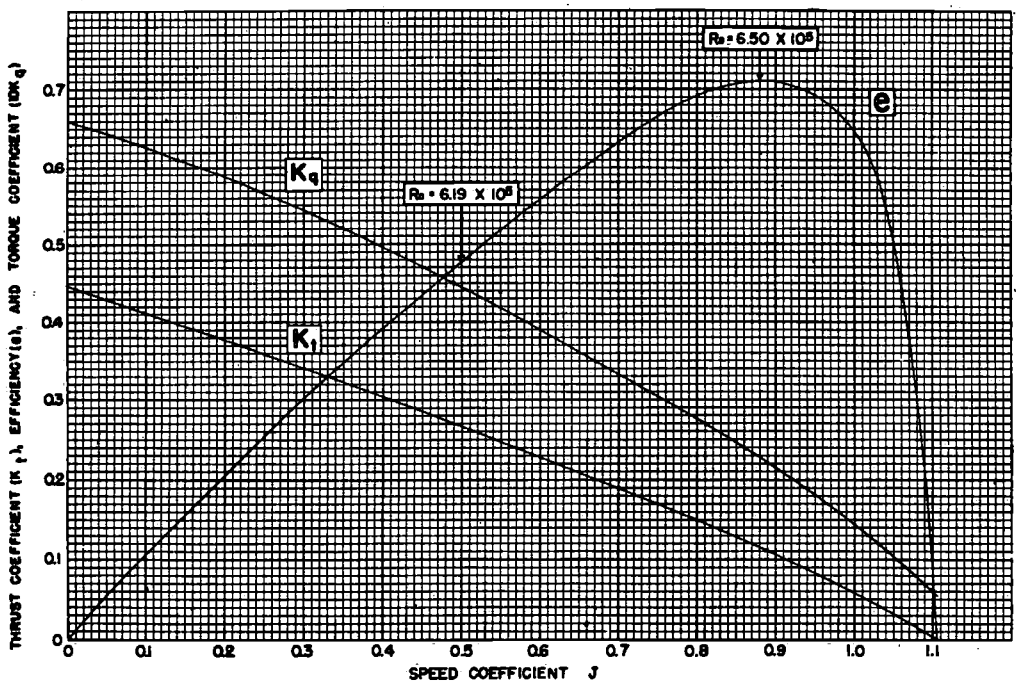

Figure 32 - Open Water Characteristics for MARINER Propeller

DISTRIBUTION LIST

Rear-Admiral J. Dieudonne
Institut De Recherches De La
Construction Navale
47 Rue De Monceau
Paris 8, France

Dr. G. S. Firsoff
Manoeuvring Qualities Division
Frunze Street 15 Apt 168
Leningrad, USSR

Mr. N. H. Norrbin
Statens Skeppsprovningsanstalt
Gotheburg 24, Sweden

Mr. H. Thieme
Institut Fur Schiffbau
Laemmersieth 90
Hamburg 33, Germany

Mr. S. Motora
Department of Naval Architecture
Faculty of Engineering
University of Tokyo
1 Motofuji-Cho Bunkyo-Ku
Tokyo, Japan

Mr. A. J. Vosper
Admiralty Experiment Works
Haslar
Gosport, Hants

Mr. V. A. Olson
Technical Administrator
Society of Naval Architecture
and Marine Eng.
74 Trinity Place
New York 6, New York

Prof. M. A. Abkowitz
Department of Naval Architecture
and Marine Engineering
Massachusetts Institute of Technology
Cambridge 39, Massachusetts

Mr. Thomas Noble
Sperry Piedmont Company
Charlottesville, Virginia

Mr. Abraham Taplin
Naval Ship Systems Command
Code 6442
Department of the Navy
Washington, D.C. 20360

Mr. Robert J. Taylor
Construction & Development Division
Tanker Department
Esso International, Inc.
Room 2640, 15 W. 51 Street
New York, New York

Mr. Seth Hawkins
Robert Taggart, Inc.
Marine Sciences Building
3930 Walnut Street
Fairfax, Virginia

Dr. Milton Martin
Principal Research Scientist
Hydronautics, Inc.
Pindell School Road
Howard County, Laurel, Md.

Mr. A. Suarez
Davidson Laboratory
Stevens Institute of Technology
Hoboken, New Jersey

Prof. A. G. Strandhagen
University of Notre Dame
Dept. of Engineering Science
Notre Dame, Indiana

Mr. Barry J. Connell
Assistant Director of Engineering
Research and Development
Grace Line Inc.
Grace Line Terminal
Pier 57
New York 11, New York

Mr. James H. Robinson
Assistant to the Naval Architect
Newport News Shipbuilding and Dry
Dock Company
Newport News, Virginia

Mr. C. L. Crane
Stevens Institute of Technology
Davidson Laboratory
Castle Point Station
Hoboken, New Jersey

State University
Buenos Aires, Argentina

Hydrodynamics Laboratory
University of Sydney
Sydney, New South Wales

University of Adelaide
Adelaide, South Australia

Schiffbautechnische Versuchs-Anstalt
in Wien
Brigittenauerlande 256, A-1200 Wien
Austria

Department of Naval Architecture
University
Josef Plateaustraat, 22, Gent
Belgium

Instituto de Pesquisas Technologicas
Praco Cel Fernando Prestes 110
Caixa Postal 7141, Sau Paulo
Brazil

Head of Ship Section, Building M-22
National Research Council
Montreal Rd., Ottawa 2, Canada

Hydro-og Aerodynamisk Laboratorium
Hjertekaersvej 99, Lyngby
Denmark

Finland Institute of Technology
Eriksgatan 56, Helsinki
Finland

Directeur du Bassin d'Essais des Carénes
6, Boulevard Victor, Paris 15 ème
France

Institut de Recherches de la Construction Navale
47 Rue de Monceau, Paris 8, France

Institut für Theorie des Schiffes
Technische Fäkultat der Universität Rostock
25 Rostock, Albert-Einstein-Str
East Germany

Schiffbau Versuchsanstalt
Stuhlinger Strasse 6, Berlin-Karlshorst
East Germany

Institut fur Schiffbau
Schiffbau-Versuchsanstalt
DDR-1157-Berlin-Karlshorst
Stuhlinger Str 6
East Germany

Technische Universitat Berlin
1 Berlin 12, Hardenbergstrasse 34
West Germany

Bersuchsanstalt für Binnenschiffbau E v,
Oststrasse 77, Duisburg
West Germany

Institut fur Schiffbau der Universitat
Hamburg
Lammersieth 90, Hamburg 33, Germany

Lehrstuhl für Schiffshydrodynamik
Technische Universitat Berlin
1 Berlin 12 (Charlottenburg)
Hardenbergstrasse 34
West Germany

Hamburgische Schiffbau-Versuchsanstalt
Bramfelder Str. 164, 2 Hamburg 33
West Germany

Versuchsanstalt für Wasserbau und Schiffbau
1 Berlin 12, Gertenufer (Schleuseninsel)
West Germany

Hamburgische Schiffbau-Versuchsanstalt
Bramfelder Str. 164, 2 Hamburg 33
West Germany

Institut für Schiffbau der Universität Hamburg
Lammersieth 90, Hamburg 33
West Germany

Institut für Schiffbau der Universität Hamburg
Lammersieth 90, 2 Hamburg 33
West Germany

Central Water and Power Research Station
20 Bombay-Poona Rd., Poona 3
India

Indian Institute of Technology
Kharagpur, India

President of Instituto Nazionale per Studi ed Esperienze di Architettura Navale
2-Via del Fagutale-ROMA
Italy

Director, Instituto Nazionale per Studi ed Esperienze di Architettura Navale
60, Via Corrado Segrè, Roma
Italy

Director, Tunnel Idrodinamico Marina
Ministero Difesa Marina-Maricominav-
Roma, Italy

Dept. of Mechanical Engineering
Defense Academy, Obaradai,
Yokohama-shi, Japan

Department of Naval Architecture
Kyushu University
Hakozaki-cho, Fukuoka-ski
Japan

Experiment Tank, University of Tokyo
Hongo 7-3, Bunkyo-ku
Tokyo, Japan

Experiment Tank
Ishikawajima-Harima Heavy Industries Co., Ltd.
Shin-Nakahara-machi, Isogo-ku,
Yokohama, Japan

Shipbuilding Research Association of Japan
Sempaku Shinko Building
35, Shiba Kotohira-cho, Minato-ku,
Tokyo, Japan

Technical Research and Development Center
Meguro Model Basin, Defense Agency
13, Mita, Meguro-ku, Tokyo, Japan

Technical Research Laboratory
Hitachi Shipbuilding & Engineering Co.
Ltd. 60, Sakurajima Kitano-cho,
Konohana-ku
Osaka, Japan

National University of Yokohama
Oooka-cho, Minato-ku, Yokohama
Japan

Manoeuvring Laboratory, Osaka University
Higashinoda-cho, Miyakojima-ku, Osaka
Japan

Institute of High Speed Mechanics
Tohoku University
Sakurakoji, Sendai, Japan

Ibaraki University
Ayukawa Tagawa-cho,
Hitachi-shi, Ibaraki
Japan

Institute of Industrial Science
University of Tokyo
10, Azabu Shin-Ryudo-cho
Minato-ku, Tokyo
Japan

Mitsubishi Experimental Tank
Mitsubishi Heavy Industries, Ltd
Akunoura, Nagasaki
Japan

Research Institute for Applied Mechanics
Kyushu University
Hakozaki-machi, Fukuoka-shi
Japan

Nippon Kaiji Kyokai
1, Akasaka Fukuyoshi-cho,
Minato-ku, Tokyo
Japan

Ship Dynamics Division
Ship Research Institute
700, Shinkawa, Mitaka-shi,
Tokyo, Japan

Ship Model Towing Tank
College of Engineering,
Soeul National University
Soeul
Valltroppsgatan 5A,
V. Frölunda, Sweden

Delft Shipbuilding Laboratory
Technological University
Mekelweg 2, Delft
Netherlands

Netherlands Ship Model Basin
Haagsteeg 2, Wageningen, Holland
Netherlands

Skipsmodelltanken, Trondheim
Norway

Towing Tank
Politechnika Gdanska
Gdansk, Poland

Canal de Experiencias Hidrolinamicas
El Pardo, Madrid
Spain

Inst. for Teknisk Hydromekanik
Kungl. Tekniska Hogskolan,
Stokholm 70, Sweden

Statens Skeppsprovingsanstalt
Box 24001
Goteborg 24, Sweden

Institute for Skeppshydromekanik
Chalmers Tekniska Hogskola
Göteborg, Sweden

Shipbuilding Institute
Technical University Gümüssuyu,
Istanbul, Turkey

Kryloff Shipbuilding Research Institute
Leningrad M 158
USSR

Admiralty Research Laboratory
Teddington, Middlesex
United Kingdom

Chief, Experimental Engineer
The British Ship Research Association
Prince Consort House, 27/29
Albert Embankment, London S.E. 1
United Kingdom

Department of Naval Architecture
The University, Newcastle-upon-Tyne
United Kingdom

Department of Naval Architecture
The University, Glasgow W2,
Scotland

Experiment Tank, Vickers Ltd.,
222, London R., St. Albans,
Hertfordshire
United Kingdom

National Physical Laboratory
Faggs Road, Feltham, Middlesex
United Kingdom

Admiralty Experiment Works
Haslar, Gosport, Hants.
United Kingdom

Davidson Laboratory
Stevens Institute of Technology
711 Hudson Street
Hoboken, New Jersey

Department of Naval Architecture
and Marine Engineering
University of Michigan
450 West Engineering Building
Ann Arbor, Michigan 48104

Hydronautics, Inc.
Pindell School Road
Laurel, Maryland

Hydraulic Laboratory
Newport News Shipbuilding and Dry Dock Co.
Newport News, Virginia

U.S. Naval Ordnance Test Station
(Code P807)
3202 E. Foothill Blvd.
Pasadena, California

Oceanics, Inc.
Technical Industrial Park
Plainview, New York 11803

Institute of Hydraulic Research
The University of Iowa
Iowa City, Iowa

Webb Institute of Naval Architecture
Crescent Beach Road, Glen Cove
New York 11542

St. Anthony Falls Hydraulic Laboratory
Mississippi River at 3rd Avenue S.E.
Minneapolis, Minnesota 55414

University of California
Berkeley, California 94720

Department of Naval Architecture
University of Zagreb
Rooseveltov Trg 6, Zagreb

Technion Towing Tank
Israel Institute of Technology
Hydraulics Laboratory, Haifa
Skipsmodelltanken
Trondheim, Norway